

Formation of Rack- and Grid-Type Metallosupramolecular Architectures and Generation of Molecular Motion by Reversible Uncoiling of Helical Ligand Strands

Adrian-Mihail Stadler,^[a] Nathalie Kyritsakas,^[b] Roland Graff,^[c] and Jean-Marie Lehn*^[a]

Abstract: The interaction of appropriate metal ions (Pb^{II} , Zn^{II}) with helical ligand strands, obtained by hydrazone polycondensation, generates polymetallic supramolecular architectures of rack and grid types, by uncoiling of the ligand. The interconversion between the helical free ligand and the linearly extended ligand in the complexes produces reversible ion-induced, nanomechanical molecular motions of large amplitude. It has been integrated in an acid–base neutralisation fuelled process, which links the extension/contraction of the ligand strands to alternating changes in pH.

Keywords: supramolecular chemistry • acid/base modulated motions • helical ligands • molecular motions • molecular muscles

Introduction

The present interest in molecular and supramolecular systems undergoing dynamic structural changes, induced by internal or external physical or chemical stimuli, rests on the important role of these processes in biological systems as well as on the potential ability to realize artificial nanoscale mechanical devices.^[1] On the other hand, there is intense activity on the controlled folding of molecular strands, in particular into helical forms.^[2] These two areas are brought together in the generation of a two-stroke linear motor type motion by chemically fuelled extension–contraction of helically folded molecular strands (**H**) undergoing reversible uncoiling/coiling upon metal ion binding and release^[3] ($\text{H} \rightleftharpoons \text{L}$ interconversion, Figure 1). Such a process has been achieved on binding of lead(II) ions to helical polyheterocyclic li-

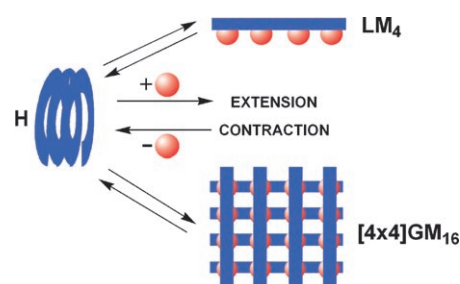


Figure 1. Uncoiling/coiling dynamic behaviour of a helical ligand; metal ion binding and release induces extension/contraction motion between a helical ligand **H** and its complexed linear form **L** in a rack-type^[3,6] LM_4 or a $[4 \times 4]$ grid-type^[5] GM_{16} architecture.

gands,^[3] based on helicity enforcing pyridine–pyrimidine (py–pym) sequences.^[4] A third attractive feature is that such ligands also undergo self-assembly with suitable metal ions to yield multinuclear grid-type (**G**) metallosupramolecular architectures;^[5] such $\text{H} \rightleftharpoons \text{G}$ interconversion (Figure 1) may also be considered to generate two-dimensional motions by extension of the molecular strand along two perpendicular directions.^[5d]

It has recently been shown that isomorphous replacement of a pyridine unit by a hydrazone (hyz) group provides very efficient synthetic access to extended helical ligand strands,^[1,8a] even up to the polymeric level.^[8b] One may expect that such ligands will also be able to undergo large amplitude extension/contraction motions as well as self-assembly into grid-type arrays upon metal ion binding. Like

[a] Dr. A.-M. Stadler, Prof. Dr. J.-M. Lehn
Institut de Science et d'Ingénierie Supramoléculaires
Université Louis Pasteur
8 Allée Gaspard Monge, 67000 Strasbourg (France)
Fax: (+33)390-245-140
E-mail: lehn@isis.u-strasbg.fr

[b] N. Kyritsakas
Service Commun de Rayons X, Institut Le Bel
Université Louis Pasteur
4 Rue Blaise Pascal, 67000 Strasbourg (France)

[c] Dr. R. Graff
Service Commun de RMN, Faculté de Chimie
Université Louis Pasteur
1 rue Blaise Pascal, 67000 Strasbourg (France)

the py-pym unit, the hydrazone-pyrimidine (hyz-pym) group is a helicity codon, inducing helical folding into molecular strands composed of (hyz-pym)_n sequences.^[7,8] Binding of a metal ion to a hyz-pym unit leads to a rotation around the bond connecting the hyz and pym groups, so that two such rotations in a β-turn shaped pym-hyz-pym sequence generates a linear terpyridine (terpy) type group on complexation of a suitable metal ion (Figure 2). Thus, the complexed unit (hyz-pym, ion) may be considered as a *linearity codon*.

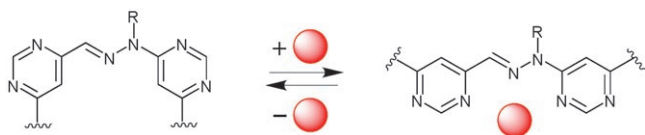
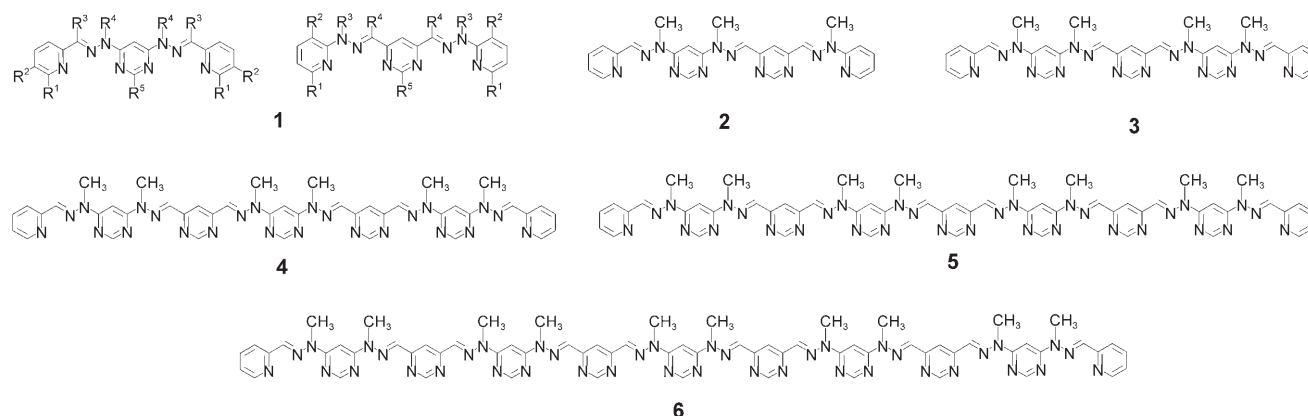


Figure 2. Conversion of the pym-hyz-pym β-turn form of the free ligand to an extended, linear shape of the ligand (right) upon binding of a metal ion.

We herewith report that the helical molecular strands **1–6**^[8a] (Scheme 1) containing from two to ten terpy-type (pym-hyz-pym) subunits, indeed undergo uncoiling with formation of the linear, rack-type^[3,6] complexes **1LM**₂–**6LM**₁₀, as well as self-assembly into the grid-type metallosupramolecular architectures **1GM**₄ and **3GM**₁₆. Furthermore, rever-



Scheme 1. Structures of the helical molecular strands **1–6** shown in extended uncoiled representation.

Abstract in Romanian: *Interacția anumitor ioni metalici (Pb^{II}, Zn^{II}) cu liganzi elicoidali preparați prin policondensarea unor hidrazine, conduce la deplierea ligandului, dând naștere unor arhitecturi supramoleculare de tip linear sau de tip “grilă”. Prin interconversia între ligandul elicoidal necoordinat și complexii lineari în care acesta este depliat, se produc mișcări moleculare nanomecanice, a căror amplitudine este importantă. Aceste mișcări au fost integrate în sisteme alimentate de energia de neutralizare acid-bază, corelându-se în acest mod extensia, respectiv contracția ligandului cu variațiile alternative ale pH-ului.*

sible interconversion between coiled free ligands and uncoiled ligands in the complexes generates large amplitude molecular motions.

Results and Discussion

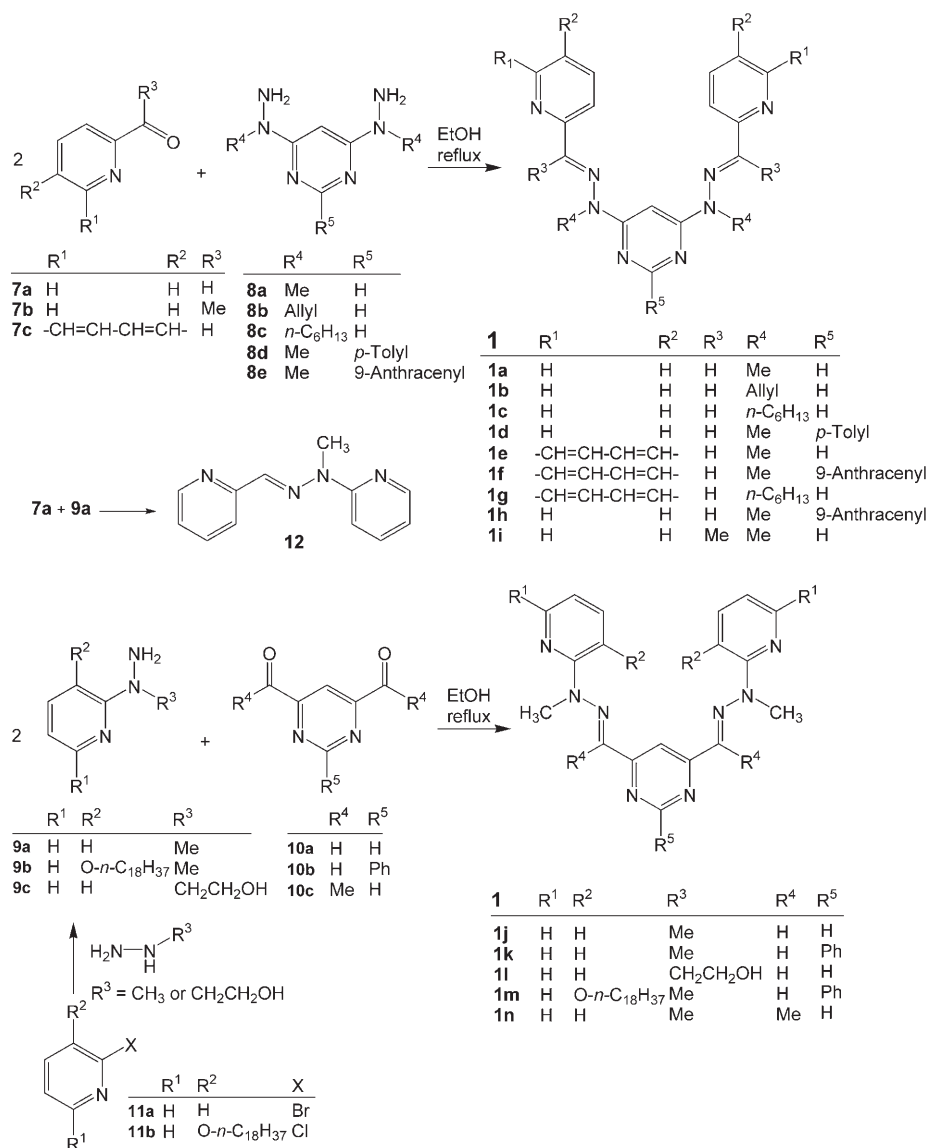
Ligand synthesis: Ligands **1–6**^[8a] were synthesized by condensation of hydrazines with carbonyl compounds, thus yielding hydrazone groups which were shown to be isomeric equivalents of a 2,6-disubstituted pyridine ring.^[7,8a] As a pym-hyz-pym sequence corresponds to a tridentate coordination site (Figure 2), each hyz group is associated with a coordination site, so that a ligand containing *n* hyz groups will be a *n*-sites ligand. Ligands **1a–1d**, **1j–1l**, **2–6** were obtained as previously described.^[8a]

Some new 2-sites ligands were prepared to test the possibilities for further functionalization (decoration) of these molecular strands (Scheme 2). The quinoline ring was introduced in ligands **1e–1g** by condensing 2-quinolinaldehyde with bis(hydrazino)pyrimidines **8a**, **8c**, and **8e** (prepared from the corresponding 4,6-dichloropyridine derivatives and the corresponding N-substituted hydrazines).

A 9-anthracenyl group was introduced in ligands **1f** and **1h** by condensation of bis(hydrazino)pyrimidine **8e** with aldehydes **7a** and **7c**.

Alkyl (or similar) groups can be attached by alkylation of the commercial 2-chloro-3-hydroxypyridine with an alkyl halide. Treatment with octadecyl bromide and potassium carbonate in DMF gave the intermediate **11b**, which by heating at reflux with methylhydrazine gave **9b**. The latter was condensed with dialdehyde **10b** to give the 2-sites ligand **1m**. The presence of two bulky OC₁₈H₃₇ groups in the latter may induce some conformational changes as confirmed by molecular modeling; however, the overall bent shape of the molecule is mainly conserved.

Finally, using the diketone **10c** in place of the corresponding dialdehyde gave ligand **1n**, in which the steric hindrance



Scheme 2. Synthesis of 1-site and 2-sites ligands.

due to the two ketimine methyl groups could impose a twist around the C–N and especially the N–N bonds, thus generating a helix with a larger step than in the case of the strand **1j**. A similar torsion is expected in the case of the ligand **1i** synthesized from 2-acetylpyridine **7b** and bis(hydrazino)pyrimidine **8a**.

Condensation of aldehyde **7a** with hydrazinopyridine **9a**, in ethanol yielded the 1-site terpy analogue **12**.

The newly prepared ligands are white, yellowish, or yellow solid materials. When large aromatic groups (such as quinoline or anthracene) are present, the melting points are generally higher than 300 °C (**1e**, **1f**, **1h**), whereas the ketone-derived ligands without such groups melt around 130–150 °C (**1i**, **1n**). A decrease of the melting point is produced by the introduction of two long alkyl chains: hexyl (m.p.: **1e**, 315 °C; **1g**, 196 °C) or octadecyl (m.p.: **1k**, 260 °C;^[8a] **1m**, 64 °C).

Preparation of metal ion complexes:

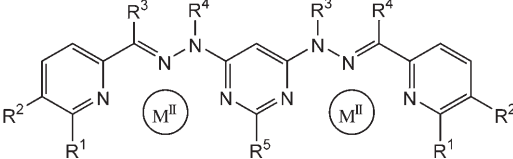
The metal ion complexes were obtained by treatment of a given ligand **1–6** with the triflate of the divalent metal ion in the corresponding molar ratio, in an appropriate solvent or mixture of solvents. For a *n*-sites helical ligand strand **1–6**, adding *n* or more equivalents of lead(II) or zinc(II) triflate generated the corresponding stick-like, linear complexes **1LM₂–6LM₁₀** (Table 1, Figure 3). When a ligand presents (as, for example, **1f** or **1h**) bulky groups making the access of metal ions difficult at the coordination sites, an excess of triflate should be used. For several 2-sites ligands **1**, the grid-like structure **1GM₄** (M^{II} = Zn^{II}, Pb^{II}) could be obtained by treating the ligand with lead(II) or zinc(II) triflate in molar ratio 1:1 (Table 2). Reacting the 4-sites ligand (**3**) with lead(II) triflate in a 1:2 molar ratio gave the [4 × 4] grid architecture **3GPb₁₆**.

The complexation studies were carried out in polar solvents, preferentially in acetonitrile or nitromethane. Thus, treatment of a suspension of a given ligand in acetonitrile or nitromethane with the corresponding quantity of metal salt led to dissolution and to formation of the complexes.

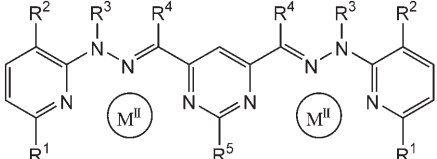
The complexes are insoluble in benzene, diethyl ether, or diisopropyl ether, chloroform, or dichloromethane. The use of mixtures of acetonitrile or nitromethane and chloroform in the appropriate v/v ratio allowed the solubilization of both ligand and complex. However, when the complex has a too high charge, the solubilization in a mixture of solvents (acetonitrile or nitromethane and chloroform) may be very difficult or impossible.

All linear complexes **1LM₂–6LM₁₀** were formed immediately by combination of the ligand with lead(II) or zinc(II) triflate in the appropriate solvent, generally at room temperature or, in several cases, by heating to 40–50 °C (to facilitate the dissolution of the ligand). The same holds for the [2 × 2] grid-type complexes **1GM₄**. The formation of the [4 × 4] grid-type complexes **3GPb₁₆** from one equivalent of **3** and two equivalents of lead(II) triflate is accelerated by heating the mixture at 40–45 °C in nitromethane or acetonitrile.

Table 1. Linear dinuclear complexes prepared with the 2-sites ligands **1** ($1:M^{II} = 1:2$, $M^{II} = Pb^{II}$ or Zn^{II}).

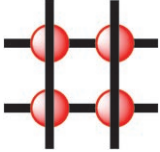


1	R ¹	R ²	R ³	R ⁴	R ⁵	M ^{II}	1LM₂	X-ray
1a	H	H	H	Me	H	Pb ^{II}	1aLPb₂	+
1b	H	H	H	Allyl	H	Pb ^{II}	1bLPb₂	
1c	H	H	H	<i>n</i> -C ₆ H ₁₃	H	Pb ^{II}	1cLPb₂	
1d	H	H	H	Me	<i>p</i> -Tolyl	Pb ^{II}	1dLPb₂	
1e		-CH=CH-CH=CH-	H	Me	H	Pb ^{II}	1eLPb₂	+
1f		-CH=CH-CH=CH-	H	Me	9-Anthracenyl	Pb ^{II}	1fLPb₂	+
1g		-CH=CH-CH=CH-	H	<i>n</i> -C ₆ H ₁₃	H	Pb ^{II}	1gLPb₂	
1h	H	H	H	Me	9-Anthracenyl	Pb ^{II}	1hLPb₂	
1i	H	H	Me	Me	H	Pb ^{II}	1iLPb₂	
1a	H	H	H	Me	H	Zn ^{II}	1aLZn₂	
1e		-CH=CH-CH=CH-	H	Me	H	Zn ^{II}	1eLZn₂	+
1g		-CH=CH-CH=CH-	H	<i>n</i> -C ₆ H ₁₃	H	Zn ^{II}	1gLZn₂	
1i	H	H	Me	Me	H	Zn ^{II}	1iLZn₂	



1	R ¹	R ²	R ³	R ⁴	R ⁵	M ^{II}	1LM₂	X-ray
1j	H	H	Me	H	H	Pb ^{II}	1jLPb₂	+
1k	H	H	Me	H	Ph	Pb ^{II}	1kLPb₂	+
1l	H	H	CH ₂ CH ₂ OH	H	H	Pb ^{II}	1lLPb₂	+
1m	H	<i>O</i> - <i>n</i> -C ₁₈ H ₃₇	Me	H	Ph	Pb ^{II}	1mLPb₂	
1n	H	H	Me	Me	H	Pb ^{II}	1nLPb₂	
1j	H	H	Me	H	H	Zn ^{II}	1jLZn₂	
1n	H	H	Me	Me	H	Zn ^{II}	1nLZn₂	

Table 2. [2×2] grid-type complexes prepared with the 2-sites ligands **1** ($1:M^{II} = 1:1$, $M^{II} = Pb^{II}$ or Zn^{II}).



1	M ^{II}	1M₄	X-ray
1a	Pb ^{II}	1aGPb₄	+
1a	Zn ^{II}	1aGZn₄	
1j	Zn ^{II}	1jGZn₄	
1m	Zn ^{II}	1mGZn₄	

NMR spectroscopic and structural features of the complexes:

¹H NMR studies of the complexation showed that coordination of metal ions increased the chemical shift of the protons of the terminal pyridine rings, with respect to the free ligand. This is mainly due to the binding of metal ions to the nitrogen atoms, thus diminishing the electronic density of the rings; in the case of ligands having more than two sites, this also results from a stacking-induced shielding effect in the folded ligands, which disappears on unfolding

by coordination of metal ions. In the case of the pyrimidine unit derived from a bis(hydrazino)pyrimidine, the proton on C5 has a higher chemical shift in the ligand than in the complex. This could be related to the proximity, in the case of the ligand, of this proton and the two C=N- bonds of the hydrazone groups, which have a deshielding effect, due to magnetic anisotropy and to the lone pair of the N atom. On formation of the complex, the N-C₄_{pym} bond (as well as the N-C₆_{pym} bond) rotates, positioning the N-CH₃ group in the location of a C=N bond, so that the chemical shift of this proton decreases. Thus, the increase of the chemical shift of the proton signals of the terminal pyridine rings (especially the two C4 and C5 proton triplets), as well as the decrease of the shift of the C5 proton of the pyrimidine ring are indicative of the coordination of the metal ion to the ligand strand, to form a linear or a grid complex.

In the case of 2-sites ligands **1**, the difference between a grid and a linear complex lies mainly in the fact that the chemical shifts of the protons are generally lower for the grids due to shielding caused by the proximity of the ligands (see also Figure 10 and 13). The ¹H NMR spectrum of the [4×4] grid **3GPb₁₆** displays signals for two different, internal and external, coordinated unfolded ligands (Figure 4).

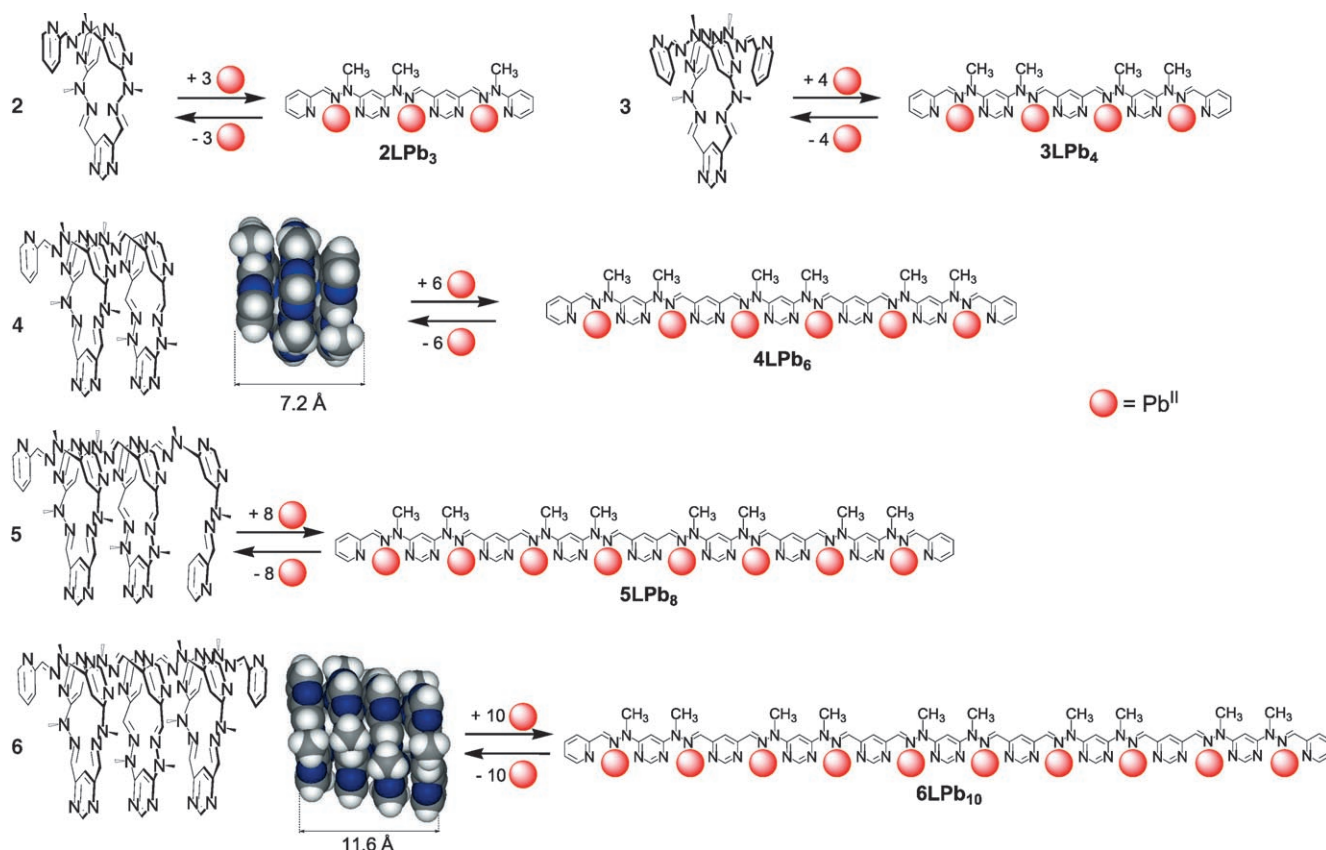


Figure 3. Generation of linear rack-type complexes $1LM_n$ ($n=2, 3, 4, 6, 8, 10$) by uncoiling of the helical ligand strands **2–6** on metal ion binding. The space-filling representations of **4** and **6** correspond to their crystal structures.^[8a]

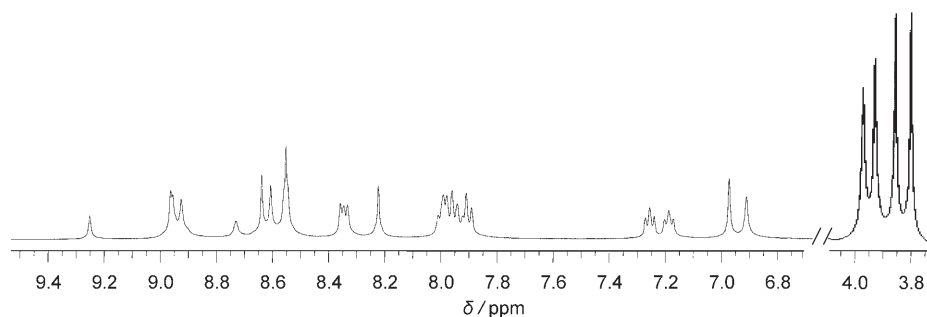


Figure 4. 400 MHz ^1H NMR spectrum of the $[4 \times 4]$ grid type complex $3GPb_6$ (solvent CD_3NO_2).

For the $[2 \times 2]$ grid $1mGZn_4$ the protons of the phenyl ring show widely different chemical shifts: $\delta=8.12, 7.64, 7.09, 5.88,$ and 5.58 ppm due to hindered rotation of the ring, intercalated between two ligands.^[5b]

Particularly pronounced ^1H NMR changes occur on uncoiling of the folded 4-turns, 10-sites ligand **6**^[8a] on formation of the extended rack $6LPb_{10}$ (Figure 5). The spectrum of the ligand is markedly spread out due to the effect of both uncoiling and metal ion binding.

NOESY and ROESY ^1H NMR data agree with the expected linear shape of the ligands in the complexes. The NOE correlations are diagnostic of the geometry change in

solution (for the ROESY of $6LPb_{10}$, see Figure 6b). The matrices displaying the NOE correlations between the protons of the folded uncoordinated strand and between the protons of the unfolded coordinated ligand, express the changes in the proximity of the protons, on passing from a helical to an extended shape of the ligand strand (Figure 7).

Direct observation of the ^{207}Pb NMR spectrum of complex $4LPb_6$ showed three peaks corresponding to the expected three types of lead(II) ions. The $^1\text{H}-^{207}\text{Pb}$ HMQC (Heteronuclear Multiple Quantum Correlation) data for $1jLPb_2$, $3LPb_4$, and $4LPb_6$ (Figure 6a) allowed indirect observation of respectively, one, two, and three signals in the ^{207}Pb dimension, confirming the presence of one, two, and three types of lead(II) ions. Moreover, the $^1\text{H}-^{207}\text{Pb}$ correlation traces allowed localization of the lead(II) ions in the complex.

Solid-state molecular structure of the complexes: The determination of the crystal structure of several complexes yield-

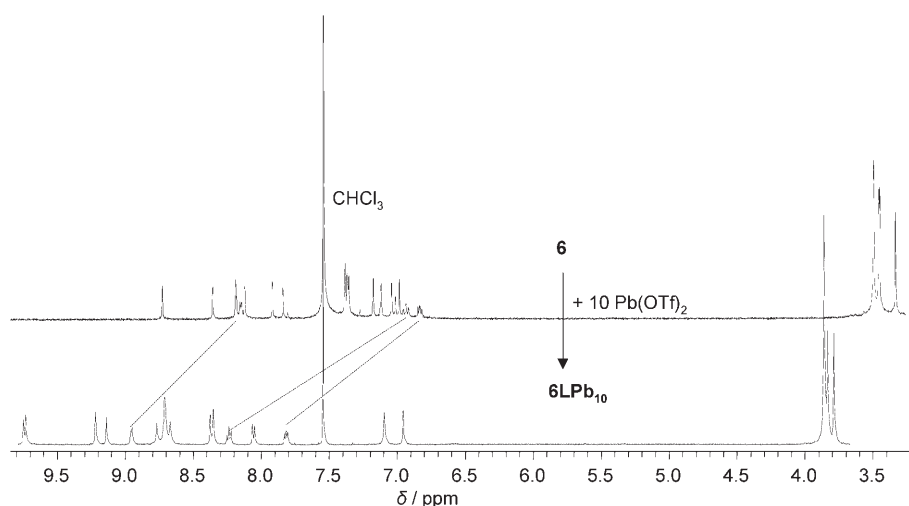


Figure 5. ^1H NMR spectral changes between the coiled ligand **6** (top, 400 MHz, $\text{CDCl}_3/\text{CD}_3\text{CN}$ 3/2) and the linear complex **6LPb₁₀** (bottom, 400 MHz, CD_3CN with CHCl_3 traces).

ed their molecular structure in the solid state. Slow diffusion of a non-solvent (diethyl ether or diisopropyl ether) into a solution of the complexes in acetonitrile or nitromethane yielded single crystals suitable for X-ray diffraction studies in the case of the compounds listed in Table 3. Representations of the molecular structure are shown in Figure 8, Figure 9, and Figure 10.

The length of the ligand strands in the dinuclear Pb^{II} linear complexes **1aLPb₂**, **1jLPb₂**, **1kLPb₂**, **1lLPb₂** is about 18 Å with pyridines as terminal groups, comparable to the previous data for linear 2-sites complexes with py-pym strands.^[3]

With terminal quinoline units, it increases to about 20 Å in **1eLPb₂**, or to 19 Å for the complex **1eLZn₂** containing the smaller Zn^{II} ions, in agreement with earlier data.^[6] For **1fLPb₂**, the angle between the planes of the anthracene and the pyrimidine groups is about 80° and for **1kLPb₂**, the angle between the phenyl ring and the pyrimidine rings is about 50°.

The intermetallic distance depends on the nature of the metal ion, of type of substitution on the pyrimidine ring separating the metal ions and of the complex (grid or rack). The shortest value is found for the smaller Zn^{II} ions in complex **1eLZn₂** (6.37 Å). The shortest Pb–Pb distance (6.48 Å; average value), is found for the grid complex **1aGPb₄**, in agreement with the fact that the grid is more compact than the rack structure.

The average Pb–N distance is 2.559 Å, larger than the Zn–N distance of 2.161 Å (see Table 4), in line with the difference of ionic radius between Pb^{II} and Zn^{II} . A second consequence of the difference of the ionic volume is that the average N–Zn–N coordination angle (74.7°) is larger than the average N–Pb–N coordination angle (63.0°, see Table 5).

The X-ray structure of the complex **1lLPb₂** shows that the OH group from the $\text{CH}_2\text{CH}_2\text{OH}$ side chain is able to coordinate a Pb^{II} ion. The average centroid-to-centroid distance between the oxygen and the lead ion is 2.55 Å, that is less

than the sum of the Pb^{II} ionic radius (1.30 Å) and the oxygen van der Waals radius (1.35 Å). The two OH groups of a ligand bind to Pb^{II} ions of two different racks, thus generating an ordered arrangement in the solid state (Figure 9).

The grid-like complex **1aGPb₄** forms a distorted square constituted by four linear organic units and four lead(II) ions (Figure 10a,b). The average length of an organic unit is 18.1 Å, comparable to that in the corresponding dinuclear complex **1aLPb₂** (about 18.2 Å, Figure 8). The four Pb^{II} ions form a distorted square, with an average Pb–Pb

internuclear distance of 6.48 Å (Table 3). The average centroid-to-centroid distance between two ligand planes is about 7.5–8 Å. Four triflate anions were found to be located in the space between two such planes, being probably responsible of the distortion from a regular square shape of the grid (Figure 10c). The packing of the grid complexes in the crystal is shown in Figure 10d.

The tetranuclear linear complex **3LPb₄** (Figure 8 and Figure 14) has a length of 32.2 Å. Two of the four Pb^{II} ions are coordinated to a water molecule. There are two types of Pb–Pb internuclear distances: 6.57–6.60 Å (comparable to those of the dinuclear complexes having the central unit derived from the bis(hydrazino)pyrimidine: **1eLPb₂**, **1fLPb₂**) and 7.19 Å (even longer than those in the dinuclear complexes having the central unit derived from the pyrimidine-dicarboxaldehyde: **1jLPb₂**, **1kLPb₂**, **1lLPb₂**).

It is worth assessing the structural consequences of the replacement of a py group in the parent complexes by a hyz unit in the present ones. The X-ray molecular structure of the lead(II) dinuclear rack **btpPb₂** obtained from $\text{Pb}(\text{OTf})_2$ and a derivative of the $\text{py}_1\text{--py}_2\text{--pym--py}_2\text{--py}_1$ 2-sites ligand **btp** ($\text{py}_1=2$ -substituted pyridine, $\text{py}_2=2$, 6-disubstituted pyridine, $\text{pym}=4,6$ -disubstituted pyrimidine) was previously determined^[3] (Figure 11).

Replacing py_2 by a hydrazone group generates two types of 2-sites symmetric isomeric ligands, because the central unit may be derived from a bis(hydrazino)pyrimidine or pyrimidine-dicarboxaldehyde, with a change of the position of the C=N bond. Consequently, this complex has to be compared to both of its hydrazone analogues **1aLPb₂** and **1jLPb₂**. The small changes observed are due to the replacement of py_2 by a hyz group, translating into a higher flexibility of the ligand. They confirm the similarity between the structural roles of the two isomeric groups. **btpPb₂** is slightly longer (18.5 Å) than **1aLPb₂** (18.2 Å) and **1jLPb₂** (18.1 Å); the Pb–Pb distance is also longer (6.94 Å) in **btpPb₂** than in the two other complexes (6.88 Å). The same

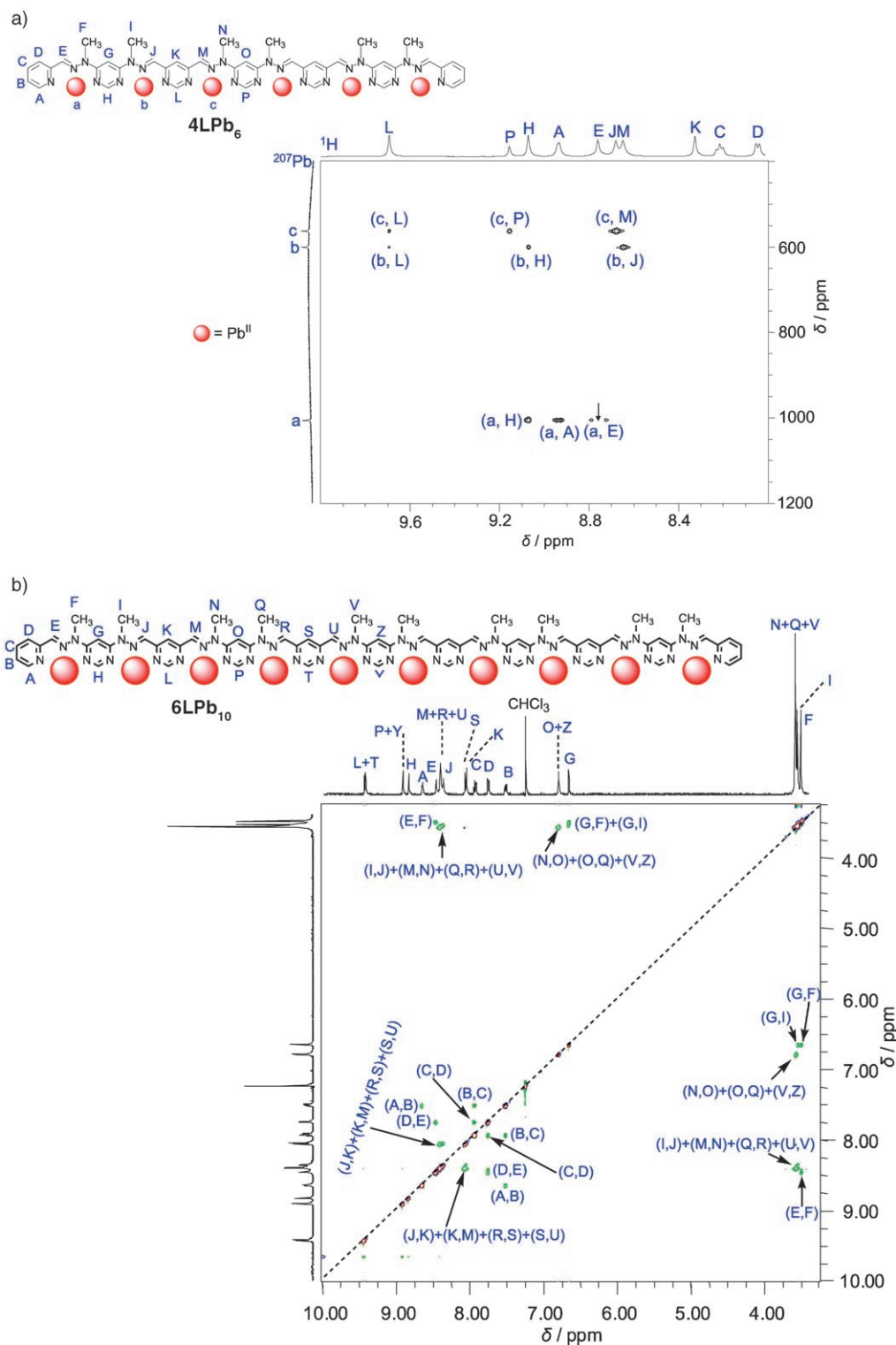


Figure 6. a) ^1H - ^{207}Pb heteronuclear multiple quantum correlation (HMQC) of **4LPb₆** (500 MHz, $\text{CD}_3\text{CN}/\text{CD}_3\text{NO}_2$ 1/1); b) ^1H - ^1H ROESY of **6LPb₁₀** (500 MHz, CD_3CN).

tendency holds for the average N-Pb-N pinching angle: 65.1° in **btpPb₂**, 62.9° in **1jLPb₂** and **1aLPb₂** (see Table 5).

Interconversion of the free ligands with linear rack-type and grid-type complexes: Treatment of **1a** in acetonitrile with

one equivalent $\text{Pb}(\text{OTf})_2$ led to the dissolution of the ligand, giving the $[2 \times 2]$ grid-type complex **1aGPb₄** (Figure 12), whose crystal structure has been determined (Figure 10). Further addition of $\text{Pb}(\text{OTf})_2$ yielded the linear rack-like complex **1aLPb₂** (Figure 12), whose crystal structure has

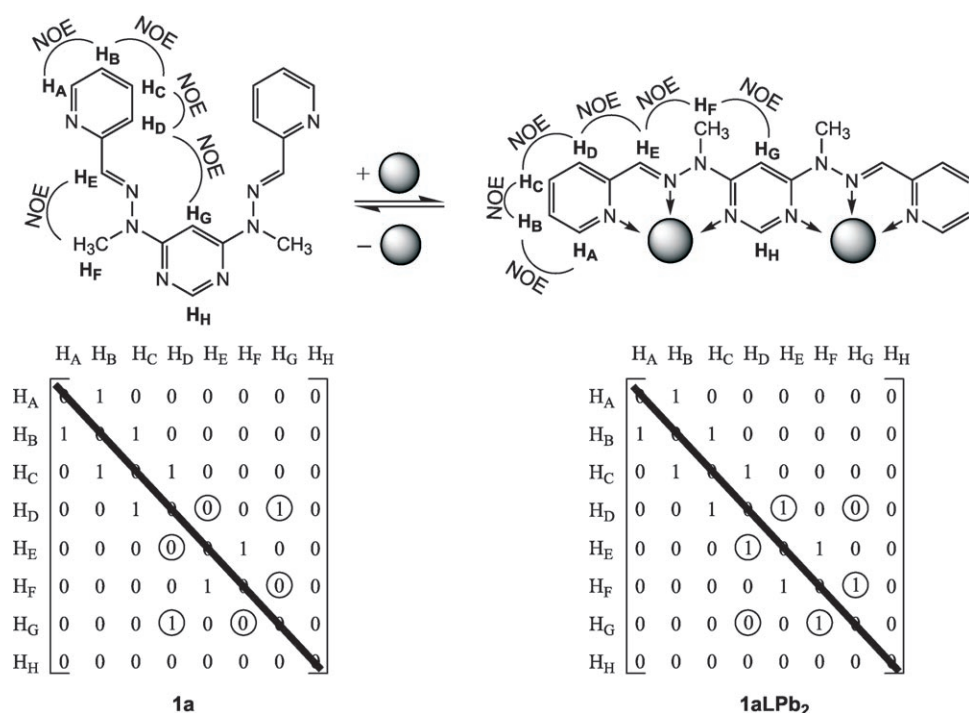


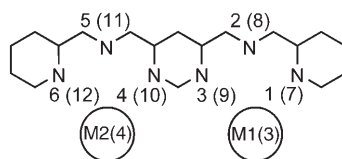
Figure 7. NOE correlation matrices (symbols: 1 = correlation; 0 = no correlation) for the curved/helical ligand strand **1a** and for the linear complex **1aLPb₂**. The encircled elements reflect the conformational changes.

Table 3. Crystallographic and molecular structural data for the crystallized complexes (all the distances are internuclear, centroid-to-centroid, distances).

Complex	Ligand	Crystal system	Space group	<i>l</i> [Å] ^[a]	M ^{II}	M ^{II} –M ^{II} distance [Å]
1aLPb₂	1a	triclinic	<i>P</i> $\bar{1}$	18.21	Pb ^{II}	6.88
1eLPb₂	1e	triclinic	<i>P</i> $\bar{1}$	20.15	Pb ^{II}	6.68
1eLZn₂	1e	triclinic	<i>P</i> $\bar{1}$	19.06	Zn ^{II}	6.37
1fLPb₂	1f	triclinic	<i>P</i> $\bar{1}$	20.03	Pb ^{II}	6.65
1jLPb₂	1j	monoclinic	<i>C</i> 12/ <i>c</i> 1	18.13	Pb ^{II}	6.88
1kLPb₂	1k	monoclinic	<i>P</i> 121/ <i>m</i> 1	18.30	Pb ^{II}	7.10
1lLPb₂	1l	orthorhombic	<i>F</i> dd2	18.26	Pb ^{II}	7.08
1aGPb₄	1a	triclinic	<i>P</i> $\bar{1}$	18.11 ^[b]	Pb ^{II}	6.48 ^[b]
3LPb₄	3	triclinic	<i>P</i> $\bar{1}$	32.29	Pb ^{II}	6.79 ^[b]

[a] *l* is the length of the ligand strand in the complex. [b] Average distance.

Table 4. M–N distances (Å) in the dinuclear complexes of ligands **1** (M^{II} = Pb^{II}, Zn^{II}). Numbering of the metal ion is the same as in the crystallographic information file (CIF).



Complex	M1–N1 Pb3–N7 ^[a]	M1–N2 Pb3–N8 ^[a]	M1–N3 Pb3–N9 ^[a]	M2–N4 Pb4–N10 ^[a]	M2–N5 Pb4–N11 ^[a]	M2–N6 Pb4–N12 ^[a]
1aLPb₂	2.487(11) 2.540(11) ^[a]	2.539(11) 2.568(10) ^[a]	2.625(11) 2.635(10) ^[a]	2.612(10) 2.654(10) ^[a]	2.573(11) 2.538(11) ^[a]	2.527(10) 2.501(11) ^[a]
1eLPb₂	2.577(5)	2.577(4)	2.579(5)	2.505(5)	2.538(5)	2.606(5)
1eLZn₂	2.201(2)	2.102(2)	2.206(2)	2.194(2)	2.089(2)	2.176(2)
1fLPb₂	2.531(6)	2.545(6)	2.542(6)	2.536(6)	2.526(7)	2.543(7)
1jLPb₂	2.506(5)	2.569(5)	2.576(4)	2.576(4)	2.569(5)	2.506(5)
1kLPb₂	2.475(7)	2.584(7)	2.663(6)	2.661(7)	2.568(7)	2.431(7)
1lLPb₂	2.495(7)	2.583(8)	2.534(8)	2.762(8)	2.608(7)	2.415(8)
btpPb₂ ^[b]	2.551	2.527	2.614	2.589	2.439	2.458

[a] Only for the complex **1aLPb₂**, presenting two kinds of racks in the asymmetric unit. [b] See discussion below.

also been determined (Table 3, Figure 8). The linear complex, as well as the grid, formed instantaneously from the ligand on addition of the corresponding quantity of Pb(OTf)₂. The process was monitored by ¹H NMR spectroscopy (Figure 13). A similar but slower, stoichiometry dependent interconversion was observed for the system **1j**, **1jGZn₄**, and **1jLZn₂**, requiring an excess of Zn(OTf)₂ (1.5 equiv) to convert the grid into the rack.

The 4-sites helical ligand **3** slowly forms the hexadecanuclear [4 × 4] grid-type complex **3GPb₁₆** on addition of two equivalents of Pb(OTf)₂ in nitromethane at 40–45 °C, as indicated by NMR investigations (¹H, COSY, ROESY; for the 1D ¹H NMR spectrum, see Figure 4), in line with earlier results.^[5c] Unfortunately, no crystals suitable for X-ray crystallography could be obtained in the present case. A solid-state structure has been described for the “parent” related complex,^[5d] confirming the nature of such a large multi-metallic metallosupramolecular architecture, formed via the self-organization of altogether 24 units in a single overall op-

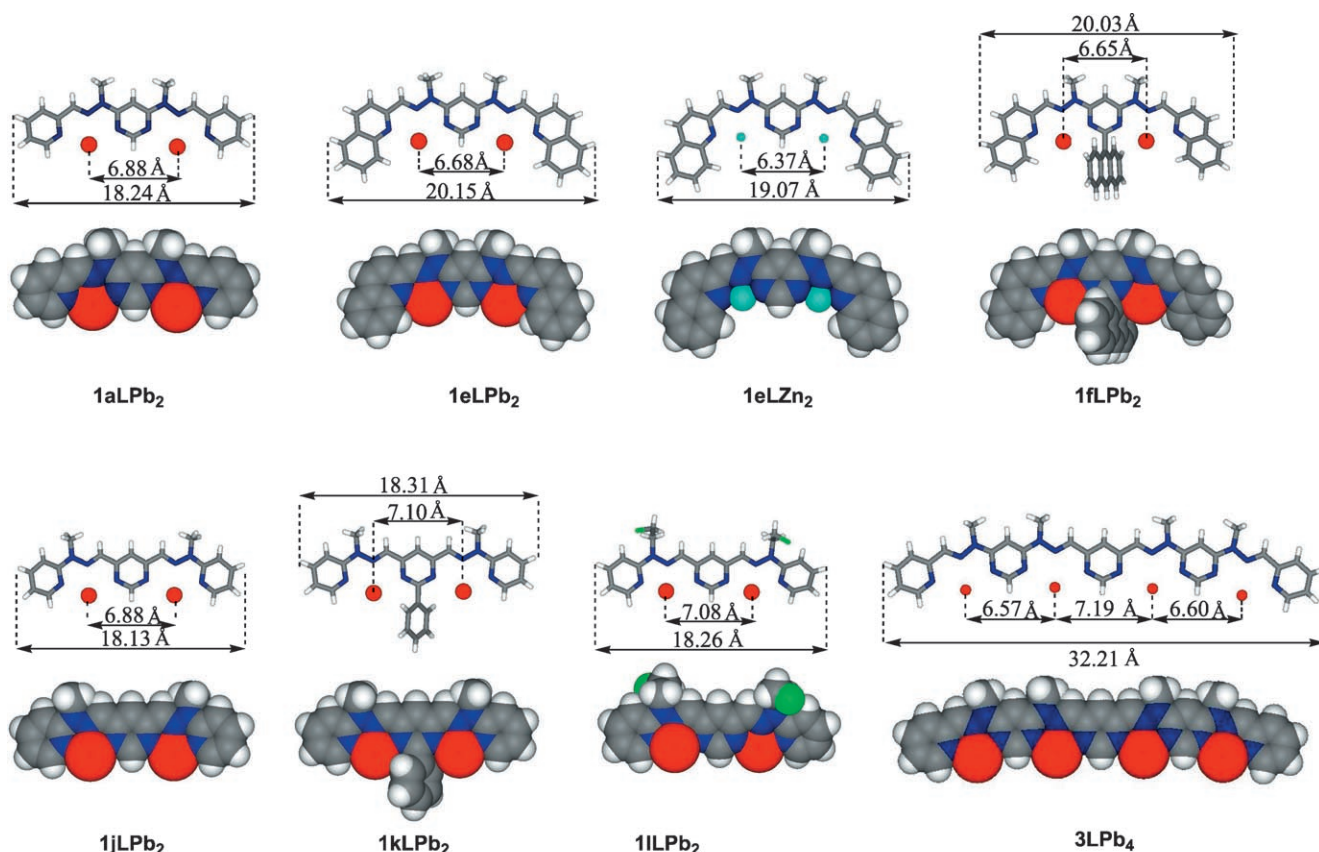


Figure 8. X-ray crystallographic molecular solid state structures of the dinuclear linear complexes **1aLPb₂**, **1eLPb₂**, **1eLZn₂**, **1fLPb₂**, **1jLPb₂**, **1kLPb₂**, **1lLPb₂**, and of the tetranuclear complex **3LPb₄**. The distances indicated are internuclear, centroid-to-centroid, distances.

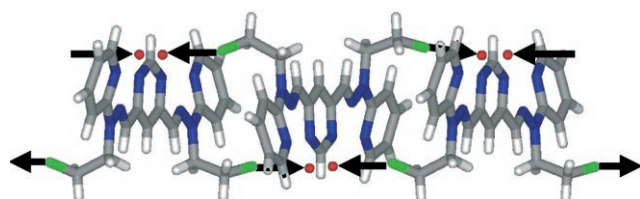


Figure 9. Ordered arrangement formed by the complex **1lLPb₂** in the solid state through Pb^{II}-oxygen inter-rack bridging coordination.

eration. Addition of two or more equivalents Pb(OTf)₂ (**3**:Pb^{II}=1:4) to **3GPb₁₆** in acetonitrile, gave the linear complex **3LPb₄** containing four bound Pb^{II} cations; its structure was confirmed by NMR studies in solution (¹H, ROESY, ¹H-²⁰⁷Pb HMQC) and by X-ray crystallography in the solid state (Figure 8). The corresponding interconversions are represented in Figure 14.

Treatment of the complexes **1aLPb₂**, **3LPb₄**, **1aGPb₄**, or **3GPb₁₆** with tren N(CH₂CH₂NH₂)₃ which binds the lead(II) ions, leads back to the helical forms **1aH** or **3H**, respectively (see below).

Table 5. N-M-N pinching angles [°] in the dinuclear complexes of ligands **1** (M^{II}=Pb^{II}, Zn^{II}). Numbering of the metal ions is the same as in the crystallographic information file (CIF).

Complex	N1-M1-N2 N7-Pb3-N8 ^[a]	N2-M1-N3 N8-Pb3-N9 ^[a]	N4-M2-N5 N10-Pb4-N11 ^[a]	N5-M2-N6 N11-Pb4-N12 ^[a]
1aLPb₂	65.5(3) 64.9(3) ^[a]	60.5(3) 59.6(3) ^[a]	61.3(3) 60.5(3) ^[a]	65.1(3) 65.9(4) ^[a]
1eLPb₂	64.7(1)	61.2(1)	62.6(2)	64.5(1)
1eLZn₂	75.9(1)	72.9(1)	73.3(1)	76.5(1)
1fLPb₂	65.5(2)	60.8(2)	61.5(2)	65.4(2)
1jLPb₂	62.3(1)	63.5(1)	63.5(1)	62.3(1)
1kLPb₂	63.2(2)	63.2(2)	62.6(2)	63.9(2)
1lLPb₂	62.9(3)	64.3(2)	61.8(2)	61.8(2)
btpPb₂ ^[b]	64.5	64.4	65.2	66.1

[a] Only for the complex **1aLPb₂**, presenting two kinds of racks in the asymmetric unit. [b] See discussion below.

Related 3-sites, 6-sites, and 8-sites ligands^[8a] similarly generate, on treatment with Pb(OTf)₂ in acetonitrile, the corresponding linear complexes (Figure 3) containing, three (¹H NMR, ROESY), six (¹H, ²⁰⁷Pb, ROESY, ¹H-²⁰⁷Pb HMQC) and eight bound Pb^{II} ions (¹H NMR, ROESY; data not shown), respectively. Finally, treating an acetonitrile suspension of the 10-sites helical ligand **6**^[8a] with excess

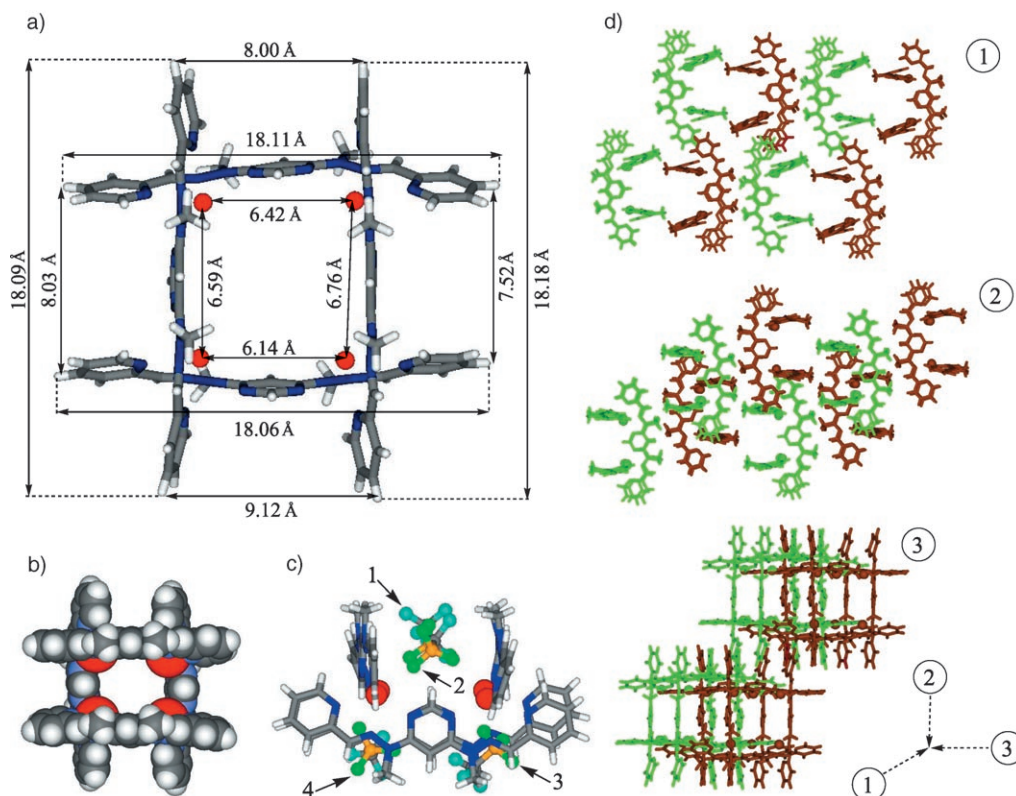


Figure 10. a) Geometric details for the molecular X-ray structure of **1aGPb₄** in the solid state (CF_3SO_3^- ions omitted for clarity); b) space-filling representation; c) side-view with the four triflate anions located in the grid, in the spaces between two ligand planes. The indicated distances are internuclear (centroid-to-centroid) distances; d) packing of the grid complexes in the crystal (anions and solvent molecules are omitted for clarity); 1 (top) and 2 (middle): view perpendicular to the planes of the ligands; 3 (bottom): view perpendicular to the transversal plane of the grid (the plane generated by the Pb^{II} cations).

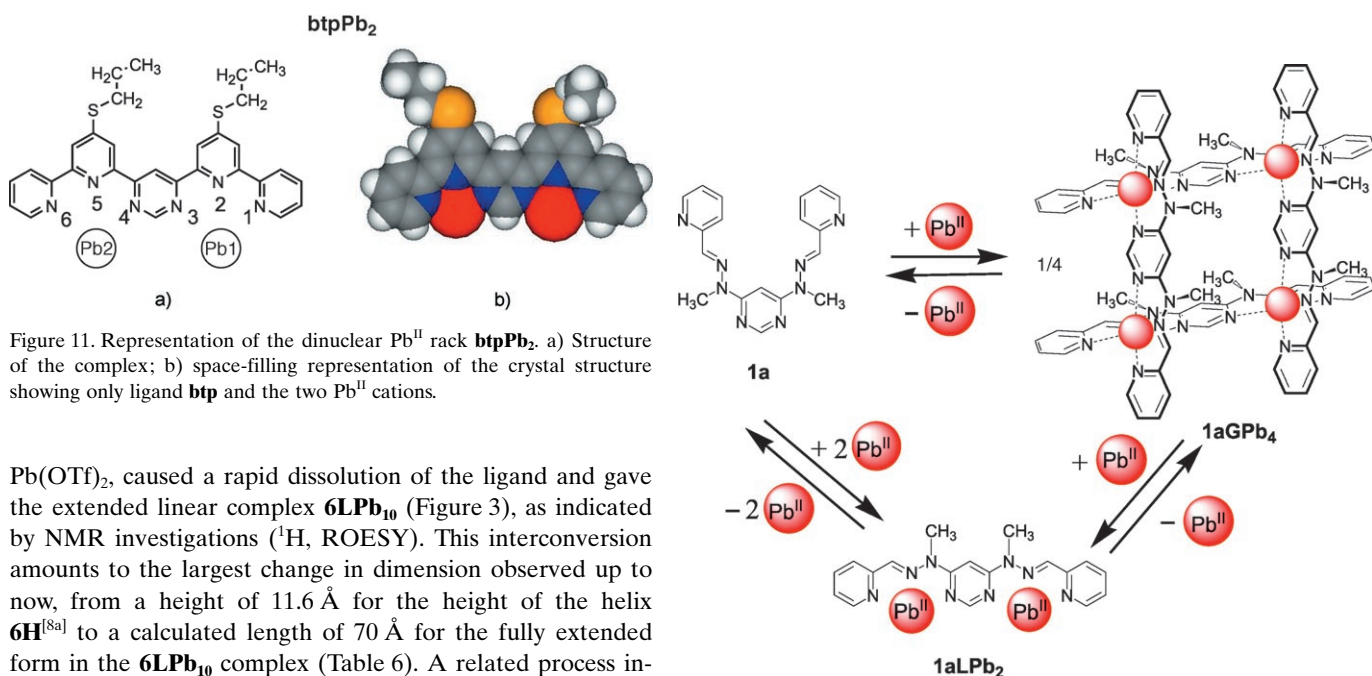


Figure 11. Representation of the dinuclear Pb^{II} rack **btpPb₂**. a) Structure of the complex; b) space-filling representation of the crystal structure showing only ligand **btp** and the two Pb^{II} cations.

$\text{Pb}(\text{OTf})_2$, caused a rapid dissolution of the ligand and gave the extended linear complex **6LPb₁₀** (Figure 3), as indicated by NMR investigations (^1H , ROESY). This interconversion amounts to the largest change in dimension observed up to now, from a height of 11.6 Å for the height of the helix **6H**^[8a] to a calculated length of 70 Å for the fully extended form in the **6LPb₁₀** complex (Table 6). A related process involving the binding of nine Pb^{II} ions gave a change from 11 Å to 60 Å.^[5] The very high nuclearity, [6×6], [8×8], and [10×10] grid-type architectures were not obtained.

Figure 12. Interconversion between the free 2-sites ligand **1a**, the [2×2] grid-type complex **1aGPb₄** and the linear complex **1aLPb₂** upon binding of lead(II) ions in different stoichiometries.

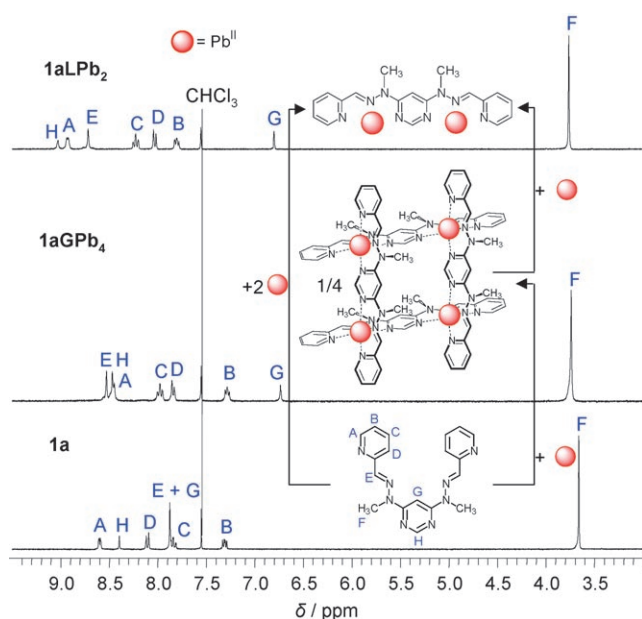


Figure 13. 300 MHz ^1H NMR observation of the conversion of the curved ligand **1a** into grid-type species **1aGPb₄**, and then into linear rack complex **1aLPb₂** by addition of one and two equivalents of $\text{Pb}(\text{OTf})_2$, respectively (solvent $\text{CD}_3\text{CN}/\text{CDCl}_3$ 4/1).

Related complexes were also prepared with $\text{Zn}(\text{OTf})_2$ and characterized in a similar manner by ^1H NMR spectroscopy: $[2 \times 2]$ grids with **1a**, **1j**, and **1m** and linear complexes with **1a**, **1e**, **1g**, **1i**, **1j**, and **1n**.

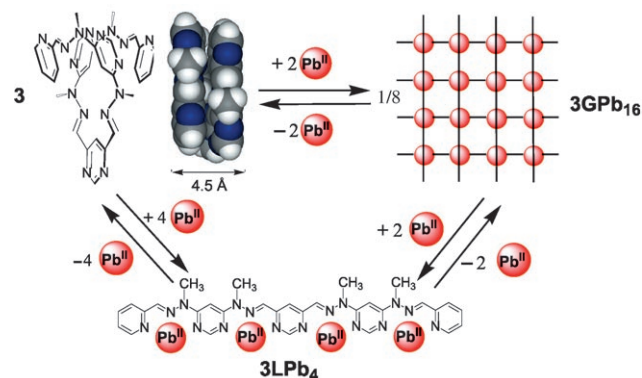


Figure 14. Interconversion between the free 4-sites helical ligand **3**, the $[4 \times 4]$ grid-type architecture **3GPb₁₆** and the linear complex **3LPb₄** upon binding of lead(II) ions in different stoichiometries.

Table 6. Amplitude (rounded values) and extension factor of the extension/contraction $\text{H} \rightleftharpoons \text{LM}_n$ motions for the molecular strands **2–6** (all distances are internuclear, centroid-to-centroid, distances).

Helical strand	h [Å] ^[a]	Method	Complex LM_n	l [Å] ^[b]	Method	Extension amplitude $\Delta l = l - h$ (Å)	Extension factor (%) $100(l - h)/h$
2	3.5	X-ray	2LPb₃	26	estimated	22	630
3	4.5	X-ray	3LPb₄	32.2	X-ray	28	620
4	7.2	X-ray	4LPb₆	46	estimated	39	540
5	10	estimated	5LPb₈	59	estimated	49	490
6	11.6	X-ray	6LPb₁₀	70	estimated	58	500

[a] h = height of the helical strand. [b] l = length of the ligand strand in the complex LM_n .

pH-fuelled nanomechanical extension/contraction motions by ligand uncoiling/coiling: Dynamic interconversion between the helical **H** and linear **L** forms of the present molecular strands (Figure 1 and Figure 3) was produced by coupling the ion binding process by ligands **1–4** to that of a competing ligand, whose ion affinity could be modulated by acid/base changes, in analogy to earlier experiments.^[3] Sequestering of lead(II) ions from the rack-type complexes **LPb_n**, containing the **L** forms of the ligands, was accomplished (in $\text{CDCl}_3/\text{CD}_3\text{CN}$) using $\text{N}(\text{CH}_2\text{CH}_2\text{NH}_2)_3$ (tren) as complexing agent.^[9] It results in spontaneous coiling of the free ligand thus liberated, to give the corresponding helical form **H**. On acidification with $\text{CF}_3\text{SO}_3\text{H}$, protonation of the complex $[\text{Pb}^{\text{II}}, \text{tren}]$ formed takes place, releasing the metal ion which binds again to the helical ligand **H** to regenerate **LPb_n**.

In the case of the 4-sites ligand **3**, the sequence of processes generated by complexation and acid-base neutralization is the following (solvent $\text{CDCl}_3/\text{CD}_3\text{CN}$ 1/1):

- uncoiling of the ligand strand by complexation with metal ions:
helical ligand **3H** + 4 Pb^{II} \rightarrow linear complex **3LPb₄**
- tren-complex formation:
linear complex **3LPb₄** + 4 tren \rightarrow helical ligand **3H** + 4 $[\text{Pb}^{\text{II}}, \text{tren}]$
- acidification and release of Pb^{II} :
helical ligand **3H** + 4 $[\text{Pb}^{\text{II}}, \text{tren}]$ + 12 H^+ \rightarrow linear complex **3LPb₄** + 4 $[\text{trenH}_3]^{3+}$
- basification and sequestering of Pb^{II} :
linear complex **3LPb₄** + 4 $[\text{trenH}_3]^{3+}$ + 12 Et_3N \rightarrow helical ligand **3H** + 4 $[\text{Pb}^{\text{II}}, \text{tren}]$ + 12 Et_3NH^+ .

In the case of ligand **4**, the pH-dependent interconversions involving the same steps were effected with lead(II) triflate and were monitored by 400 MHz ^1H NMR in a 2/3 $\text{CDCl}_3/\text{CD}_3\text{CN}$ solvent mixture for Pb^{II} . The reversibility of the phenomena and their fast rate (within the time required for recording the spectra) were indicated by NMR measurements as shown in Figure 15. The processes taking place in all these pH-induced interconversions are summarized in Figure 16 for the **4H/4LM₆** couple ($\text{M}^{\text{II}} = \text{Pb}^{\text{II}}$).

In the case of the longest strand **6** it was difficult to find a mixture of CDCl_3 and CD_3CN able to dissolve the ligand as well as the complex, so the interconversions were effected by evaporating alternatively the appropriate pure solvents.

To determine the amplitude of the extension, it is necessary to estimate the length of the strands involved in the process, taking the solid state molecular structure as basis (Figure 3, Figure 8 and Figure 14). For the **H** form of the free ligand molecules, the height of the coiled, folded strand can be determined from the X-ray

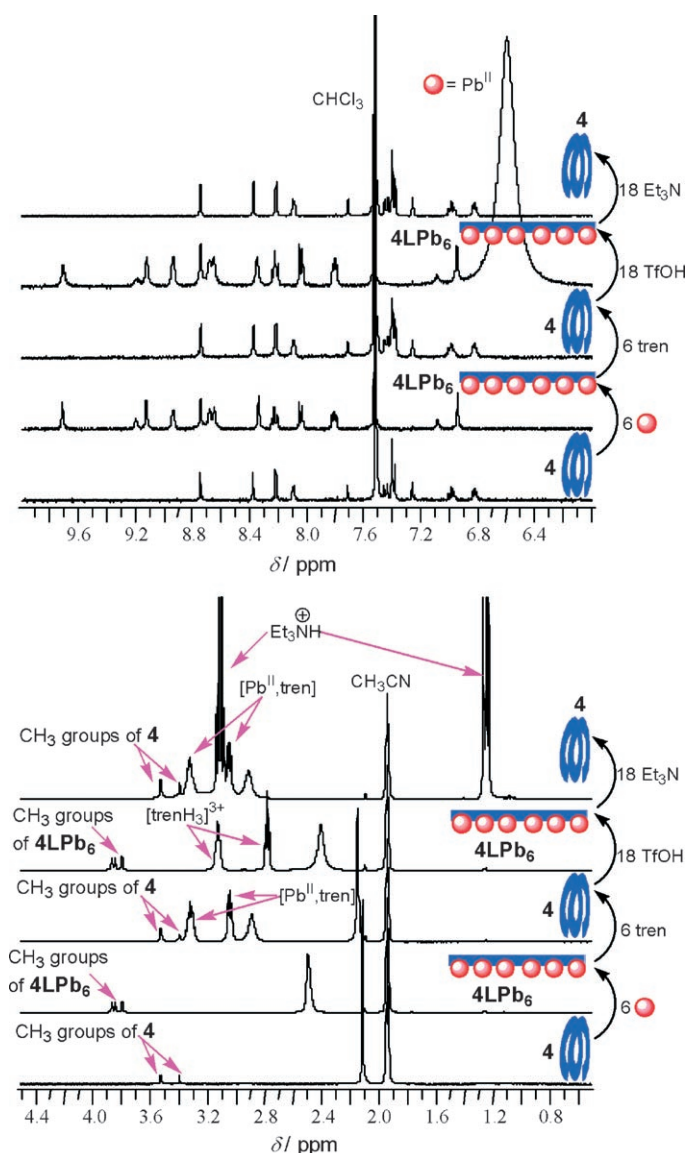


Figure 15. Proton NMR (400 MHz) observation of the reversible uncoiling/coiling structural switching between the helical ligand **4H** and the complex **4LPb₆** (in CDCl₃/CD₃CN 2/3), following the cycle displayed in Figure 16. The aromatic domain (top) of the spectra is amplified by a factor of 16 with respect to the aliphatic region (bottom). The large peak at $\delta=6.63$ ppm in the fourth spectrum is due to the presence of TfOH. Sequestering of the Pb^{II} ions from the complexes is accomplished with the competing ligand N(CH₂CH₂NH₂)₃ (tren).

data,^[8a] as the height h of the cylinder containing the molecular helix.

For the complex **LM_n** incorporating the uncoiled form of the strands, the crystallographic data for the 2- and 4-sites racks (Figure 8) can be used to estimate the length l of the other (3-, 4-, 6-, 8-, and 10-sites) linearized strands. The resulting distances and calculated amplitudes $l-h$ of the extension/contraction motions are given in Table 6 (all distances are internuclear, centroid-to-centroid, distances).

Adding sequentially tren, CF₃SO₃H and then Et₃N to the ligand/metal ion system, thus generates an alternating exten-

sion/contraction linear molecular mechanical motion of artificial muscle type.^[10] It displays very large stroke amplitudes (up to about 58 Å for **6**; extension factors $100(l-h)/h$ of about 500–600%) compared to known biological or synthetic molecular entities,^[1d] is induced by an ionic process and is fuelled by acid/base neutralization.

The extension/contraction process performed by the helical ligands **2–6** (Figure 3) on binding of metal ions, amount to a two-stroke linear motor type of nanomechanical action, fuelled by acid/base neutralization.

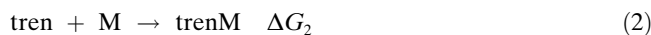
Energetic analysis of the molecular motions: Without taking into account the π - π stacking energy, the work W_n required to transform the helical ligand into its extended, linear form (Figure 17) is the total energy necessary to convert all N-C-C-N *transoid* (in the helix) conformations into *cisoid* ones. Values of 25–30 kJ mol⁻¹ have been calculated for the conversion of 2,2'-bipyridine from its *transoid* to its *cisoid* form^[11a-d] and an energy difference of about 33 kJ mol⁻¹ has been obtained for the same conversion in the py-pym case.^[11e] Assuming that a hydrazone has features comparable to a pyridine group, there are two such *transoid*-to-*cisoid* torsions (each amounting to about 30 kJ mol⁻¹) per terpy-like pym-hyz-pym coordination subunit. Thus, for a ligand having n such sites, the total molar work to be spent for fully extending the helical form to the linear one is $W_n = 60n$ kJ mol⁻¹, the molecular value being $W_{nm} = W_n/N_A$. In fact, this value of W_n is a lower limit, as the stacking energy, which should further stabilize the helical shape is not taken into account. Although these motional processes are of Brownian nature, if one wishes to translate this into the macroscopic language of force, the energy required for performing the molecular uncoiling can be used to define an average force: $F_n(\mathbf{H}, \mathbf{L}) = W_{nm}/\Delta l = W_{nm}/(l-h) = -F_n(\mathbf{L}, \mathbf{H})$, which is also the return force for the molecule to coil up from a given extended form (Figure 17). It amounts to roughly 150 pN for the five strands. The corresponding energy and force values are presented in Table 7.

One may roughly estimate the free energy of the four types of reactions taking place in the coiling/uncoiling processes (Figure 16; [Eqs. (1)–(4)]):

- ligand complexation:



- tren complexation:



- tren protonation:



- triethylamine protonation:



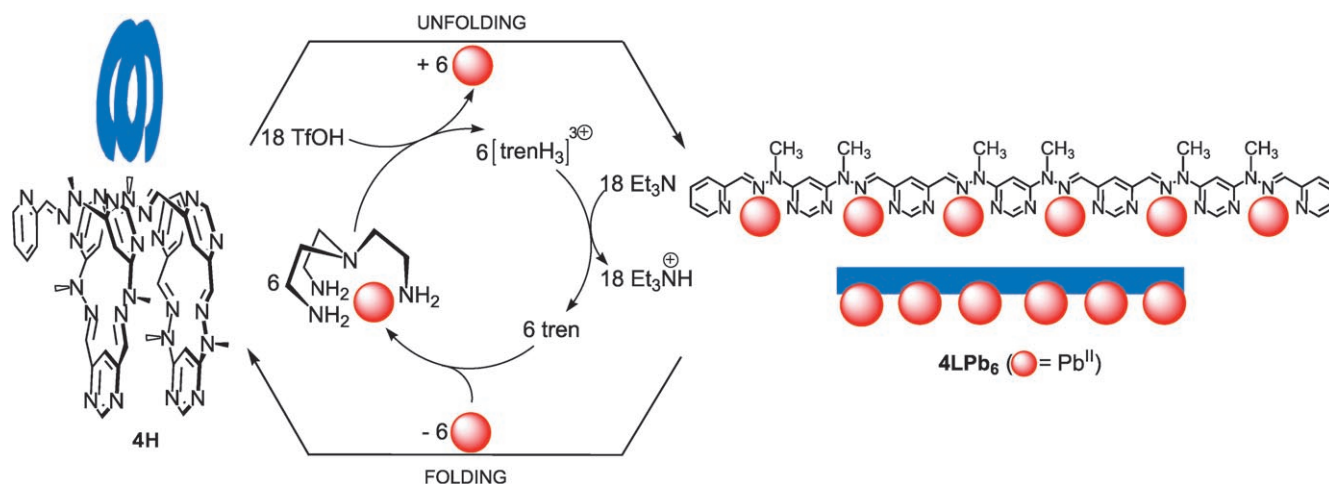


Figure 16. Acid-base fuelled reversible extension/contraction motion generated by uncoiling/coiling of a helical molecular strand (**4H**) on metal ion (Pb^{II}) binding. It is triggered by the sequential sequestering and release of the metal ions by the competing ligand tren $[\text{N}(\text{CH}_2\text{CH}_2\text{NH}_2)_3]$, induced by protonation/neutralization reactions; $\text{TfOH} = \text{CF}_3\text{SO}_3\text{H}$.

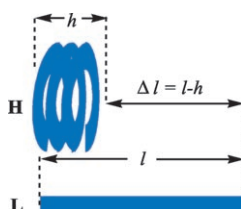


Figure 17. Geometric parameters of the conversion of a helical ligand (**H**) of height h (the height of the cylinder in which the helix can be inscribed) into its fully stretched linear form (**L**) of length l .

Table 7. Extension work and force values for the conversion $\mathbf{H} \rightleftharpoons \mathbf{L}$ conversion of the molecular strand **2–6** containing n pym-hyz-pym subunits (see Figure 17).

Ligand strand	n	$W_n = 60n$ [kJ mol ⁻¹]	$W_{nm} = 60n/N_A$ [J per molecule]	$F_n(\mathbf{H}, \mathbf{L}) =$ $W_{nm}/\Delta l$ [pN]
2	3	180	30×10^{-20}	135
3	4	240	40×10^{-20}	140
4	6	360	60×10^{-20}	155
5	8	480	80×10^{-20}	165
6	10	600	100×10^{-20}	170
average value				150

The solvent considered here is acetonitrile. The free energies for the full process were estimated for the case of lead(II). ΔG_1 is the free energy of the complexation reaction of the 1-site ligand **12** (obtained from pyridinecarboxaldehyde and 2-(methylhydrazino)pyridine; Scheme 2) with lead triflate ($n=1$) yielding the complex **12Pb**. The complexation free energy of the larger ligands was considered equal to $n\Delta G_1$ (n being the number of coordination subunits of the ligand), not taking into account the π - π stacking energy or other secondary contributions.

The complexation of the helical ligand to give the polynuclear complex can be considered as composed of two distinct processes (Figure 18):

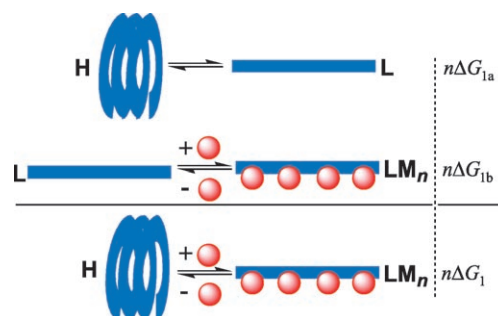


Figure 18. Thermodynamic representation of the two processes of the formation of the linear complex \mathbf{LM}_n from the helical ligand **H**: uncoiling of the helical ligand ($\mathbf{H} \rightarrow \mathbf{L}$, $n\Delta G_{1a}$) and binding of metal ions to the linear form ($\mathbf{L} + n\mathbf{M} \rightarrow \mathbf{LM}_n$, $n\Delta G_{1b}$). W_n is assumed to be a measure of $n\Delta G_{1a}$.

- the uncoiling of the ligand without coordination, to give an all-*cisoid* uncoordinated form ($\mathbf{H} \rightarrow \mathbf{L}$ energy difference W_n ; Table 7), for which the free energy is $n\Delta G_{1a} > 0$, because the coiling is spontaneous and the coiled form is the stable one;
- the binding of the metal ions to the preorganized n py-hyz-pym coordination sites of the extended form, whose free energy is $n\Delta G_{1b} < 0$.

For the molecular extension to take place, the coordination free energy of the metal cations (Pb^{II}) to the ligand strand must be larger than W_n , assuming that W_n is a measure of the free energy of the \mathbf{H} to \mathbf{L} conversion (Figure 18).

The $n\Delta G_1$ value for a n -site ligand represents the summation of the two free energies: $n\Delta G_1 = n\Delta G_{1a} + n\Delta G_{1b}$ with $n\Delta G_1 < 0$, as coordination leads to uncoiling (Figure 18).

Free enthalpy values $n\Delta G_1$ were calculated from $\Delta G_1 = -RT \ln K_1$, where K_1 is the corresponding equilibrium constant ($T=298$ K). K_1 was determined by spectrophotometric UV titration of the 1-site ligand **12** with $\text{Pb}(\text{OTf})_2$ in acetonitrile. K_3 was estimated for the reaction in acetonitrile, cor-

recting the pK_a value in water^[12] by adding an average of 7.7 units to take into account the passage from water to acetonitrile in the case of amines.^[13] K_4 was taken from the literature.^[13] The following values were obtained: $K_1=10^{8.2}M^{-1}$, $\Delta G_1=-47\text{ kJ mol}^{-1}$; $K_3=10^{52.4}M^{-3}$, $\Delta G_3=-299\text{ kJ mol}^{-1}$; $K_4=10^{18.5}M^{-1}$, $\Delta G_4=-105\text{ kJ mol}^{-1}$.

The reversible interconversion between a helical ligand strand **L** of n subunits and its linear complex **LM_n** proceeds via the following set of steps (Figure 16; $M^{II}=\text{Pb}^{II}$; [Eqs. (5)–(8)]):

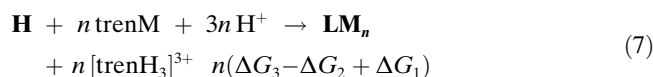
● step I:



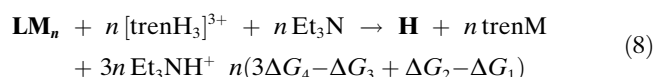
● step II:



● step III:



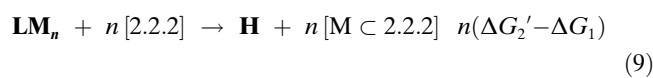
● step IV:



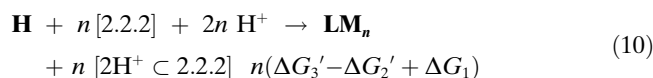
● subsequent odd and even steps are repeats of steps III and IV, respectively.

As the binding constant of Pb^{II} with tren was not available, following earlier work,^[3] we used as benchmark for thermodynamic calculations the value for the complexation of Pb^{II} with the cryptand [2.2.2]^[14a,c] ($K_2'=10^{13}M^{-1}$, $\Delta G_2'=-74\text{ kJ mol}^{-1}$; in methanol); even higher stability may be expected in a chloroform/acetonitrile mixture as well as the free energy of diprotonation^[14b,c] of this ligand ($\Delta G_3'=-112\text{ kJ mol}^{-1}$). Consequently, steps II, III, and IV are rewritten as shown in Equations (9)–(11):

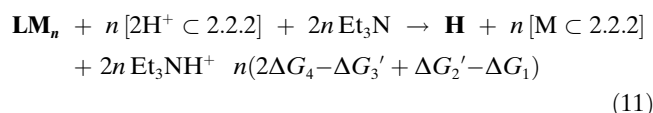
● step II:



● step III:



● step IV:



The molar values ΔG_{molar} per subunit are listed in Table 8. The corresponding molecular values $\Delta G_{\text{molecular}}$ are obtained

Table 8. Molar and molecular free energy values per coordination subunit for the steps occurring in the reversible interconversion of a helical ligand strand **H** and the corresponding linear Pb^{II} complex **LM_n** (calculations for cryptand [2.2.2] as complexing agent).

Free energy	ΔG_{molar} [kJ mol ⁻¹]	$\Delta G_{\text{molecular}}$ [J per molecule]
ΔG_1	-47	-8×10^{-20}
$\Delta G_2' - \Delta G_1$	-27	-5×10^{-20}
$\Delta G_3' - \Delta G_2' + \Delta G_1$	-85	-14×10^{-20}
$2\Delta G_4 - \Delta G_3' + \Delta G_2' - \Delta G_1$	-125	-21×10^{-20}

by dividing the molar values by Avogadro's number N_A : $\Delta G_{\text{molecular}} = \Delta G_{\text{molar}}/N_A$.

The “useful” energies, in terms of molecular mechanical motions, are those of the extensions (5) and the contractions W_n (Table 7). The available work in extension (5), $n\Delta G_1$, results from the excess of the coordination free energy of Pb^{II} over the energy required for the uncoiling of the ligand (see Table 9). The contraction energy W_n becomes available as

Table 9. Extension work and force values for the conversion $\mathbf{H} \rightleftharpoons \mathbf{LM}_n$ conversion of the molecular strand 2–6 containing n pym-hyz-pym subunits (see Figure 17).

Ligand strand	n	$-n\Delta G_1=47n$ [kJ mol ⁻¹]	$-n\Delta G_{1\text{molecular}} = -n\Delta G_1/N_A = 47n/N_A$ [J per molecule]	$F_n(\mathbf{H}, \mathbf{LM}_n) = -n\Delta G_{1\text{molecular}}/\Delta l$ [pN]
2	3	140	23×10^{-20}	105
3	4	190	31×10^{-20}	110
4	6	280	46×10^{-20}	118
5	8	375	62×10^{-20}	130
6	10	470	78×10^{-20}	134

soon as the ligand tren has sequestered the metal ions and generated the free extended strand **L**. In the language of force, the extension develops an average push $F_n(\mathbf{H}, \mathbf{LM}_n) = -n\Delta G_{1\text{molecular}}/\Delta l = -n\Delta G_{1\text{molecular}}/(l-h)$ of 120 pN per molecule (Table 9) and the contraction corresponds to a pull $F_n(\mathbf{L}, \mathbf{H})$ (Table 7).

One may note that the energies available for the “forward” ($\mathbf{H} \rightarrow \mathbf{LM}_n$) and “backward” ($\mathbf{L} \rightarrow \mathbf{H}$) motions are different as they correspond to different processes. When the complexing agent is the cryptand [2.2.2], the energy consumed in the process is that of the protonation of Et_3N , that is, $2 \times 105 = 210\text{ kJ mol}^{-1}$. The energy wasted in the linear engine motions amounts to the excess of the energy consumed over the work developed in the extension, that is, $210 - 47 \sim 163\text{ kJ mol}^{-1}$ per ligand site/metal ion bound.

A “macroscopic” way to look at the force $F_n(\mathbf{H}, \mathbf{LM}_n)$ is to consider the mass of the object that, connected to one end, would be pushed up by means of the extension of such a helical strand fixed onto a surface by its other end. Thus, $F_n(\mathbf{H}, \mathbf{LM}_n) = m \cdot g$, where $g = 9.8\text{ ms}^{-2}$. For an average value of $F_n(\mathbf{H}, \mathbf{LM}_n)$ of 120 pN we obtain $m = Fg^{-1} \approx 12\text{ ng}$. These values of the force may be compared with that of 200 pN of the calculated force developed by a molecular elevator^[15]

made of a platformlike component interlocked with a trifurcated rlglike component.

Conclusion

The efficient synthetic access to helical ligands of type **1–6**, by means of hydrazine-carbonyl condensations,^[7,8a] provides a very attractive entry into the generation of a range of novel metallosupramolecular architectures, as well as into the further exploration of chemically induced and fuelled molecular mechanical processes. In particular, these ligands allow for easy derivatization, thus opening the possibility to introduce various side group decorations, in particular biological residues, and to design integrated devices bearing functional components. Furthermore, the reversible interconversion between helically wrapped and linearly extended forms induces positional changes in the groups attached, thus modulating both their internal interactions as well as their interactions with external entities (large molecules, e.g. proteins, surfaces etc.). Such investigations are being actively pursued.

Experimental Section

Materials and general methods: The following reagents were prepared as previously described: **1a–1d**, **1j–1l**, **2–6**, **8a,c**,^[7] **9a**,^[16] **10b**,^[17] **10c**,^[18] 2-anthracenyle-4,6-dichloropyrimidine.^[19] The following reagents were purchased from commercial sources: triethylamine (Lancaster, 99%), tren (Lancaster), triflic acid (Aldrich), methylhydrazine (Fluka), 2-pyridine-carboxaldehyde (**7a**, Aldrich), 2-acetylpyridine (**7b**, Aldrich), 2-quinolinaldehyde (**7c**, Aldrich), 3-chloro-2-hydroxypyridine (Aldrich), octadecylbromide (Fluka), Zn(OTf)₂ (Aldrich), CD₃CN (Eurisotop), CD₃NO₂ (Aldrich), CDCl₃ (Eurisotop; keep on basic alumina).

500 MHz ¹H and 104.3 ²⁰⁷Pb NMR spectra were recorded on a Bruker Ultrashield Avance 500 Spectrometer, 400 MHz ¹H and 100 MHz ¹³C NMR spectra were recorded on a Bruker Ultrashield Avance 400 Spectrometer, 300 MHz ¹H and 75 MHz ¹³C NMR spectra were recorded on a Bruker AM 300 spectrometer. The solvent signal was used as an internal reference for both ¹H and ¹³C NMR spectra.^[20] For ²⁰⁷Pb the reference was Pb(OTf)₂ ($\delta = 6480.7$ ppm). The following notation is used for the ¹H NMR spectral splitting patterns: singlet (s), doublet (d), triplet (t), multiplet (m).

2D-NMR used experiments were: COSY (correlation spectroscopy), HMQC (heteronuclear multiple-quantum correlation (coherence)), NOESY (nuclear Overhauser enhancement spectroscopy or nuclear Overhauser and exchange spectroscopy), ROESY (rotating-frame Overhauser enhancement (effect) spectroscopy). Concentrated solutions of complexes (0.05–0.1 M) were used to record ²⁰⁷Pb 1D spectra or ¹H-²⁰⁷Pb HMQC.

Mass spectrometry measurements were performed by the Service de Spectrométrie de Masse, Université Louis Pasteur. Melting points were recorded on a Büchi Melting Point B-540 apparatus and are uncorrected. Microanalyses were performed by the Service Central de Microanalyse du CNRS, Faculté de Chimie, Strasbourg or at FZK, Karlsruhe.

Stability constant determination were performed with LETAGROP-SPEFO software, using data obtained by UV/Vis titration of ligand **12** with solutions of Pb(OTf)₂ in acetonitrile. UV/VIS Spectra were recorded on a Varian-Cary-3 spectrometer or on a Jasco V-560 spectrometer.

Ligand synthesis

Quinoline-2-carboxaldehyde (pyrimidine-4,6-diyl)bis(methylhydrazone) (1e): A suspension of 2-quinolinaldehyde **7c** (56 mg, 0.356 mmol) and **8a**

(30 mg, 0.179 mmol) in EtOH (10 mL) was heated to reflux for 20 h. Then, the mixture was cooled and filtered. The precipitate was washed with EtOH and dried for 10 h under high vacuum: **1e** (62 mg, 78%). Yellowish solid. M.p. 315 °C. ¹H NMR (300 MHz, CDCl₃): $\delta = 8.51$ (d, $J = 1$ Hz, 1H), 8.37 (d, $J = 8.7$ Hz, 2H), 8.22 (d, $J = 8.7$ Hz, 2H), 8.10 (d, $J = 8$ Hz, 2H), 8.07 (s, 2H), 8.04 (d, $J = 1$ Hz, 1H), 7.90 (dd, $J = 1$, 8.2 Hz, 2H), 7.77 (ddd, $J = 1.3$, 7, 8.2 Hz, 2H), 7.59 (ddd, $J = 1.3$, 7, 8 Hz, 2H), 3.77 ppm (s, 6H); ¹³C NMR (100 MHz, CDCl₃): $\delta = 162.76$, 156.93, 154.69, 136.90, 136.63, 130.38, 128.52, 127.88, 127.71, 127.14, 117.89, 117.62, 89.47, 30.11 ppm; HRMS (FAB-MS): calcd for [C₂₆H₂₂N₈+H]⁺: 447.2046; found: 447.2049; elemental analysis (%) calcd for C₂₆H₂₂N₈: C 69.94, H 4.97; found: C 69.75, H 5.13.

Quinoline-2-carboxaldehyde [2-(9-anthracenyl)-pyrimidine-4,6-diyl]bis(methylhydrazone) (1f): A suspension of **7c** (28 mg, 0.178 mmol) and **8e** (30 mg, 0.087 mmol) in EtOH (5 mL) was heated to reflux for 24 h. Then, the mixture was cooled and filtered. The precipitate was washed with EtOH and dried for 10 h under high vacuum: **1f** (28 mg, 52%). White solid. M.p. >350 °C (decomp). ¹H NMR (400 MHz, CDCl₃; the compound has a poor solubility): $\delta = 8.57$ (s, 1H), 8.47 (d, $J = 8.2$ Hz, 2H), 8.28 (d, $J = 9.1$ Hz, 2H), 8.21 (s, 1H), 8.14–8.05 (m, 6H), 7.95–7.88 (m, 4H), 7.81–7.75 (m, 3H), 7.66–7.60 (m, 2H), 7.52–7.40 (m, 4H), 3.75 ppm (s, 6H); ¹³C NMR could not be obtained due to poor solubility; FAB-MS: m/z (%): 623.0 (100) [M+H]⁺; HRMS (FAB-MS): calcd for [C₄₀H₃₀N₈+H]⁺: 623.2672; found: 623.2669.

Quinoline-2-carboxaldehyde (pyrimidine-4,6-diyl)bis(hexylhydrazone) (1g): A suspension of **7c** (31 mg, 0.197 mmol) and **8c** (30 mg, 0.097 mmol) in EtOH (5 mL) was heated to reflux for 4 h. Then, the mixture was cooled and filtered. The precipitate was washed with EtOH and dried for 10 h under high vacuum: **1g** (52 mg, 91%). White solid. M.p. 196 °C. ¹H NMR (300 MHz, CDCl₃): $\delta = 8.50$ (s, 1H), 8.34 (d, $J = 8.6$ Hz, 2H), 8.15 (d, $J = 8.6$ Hz, 2H), 8.09 (d, $J = 8.5$ Hz, 2H), 8.03 (s, 2H), 7.92 (s, 1H), 7.85 (d, $J = 8$ Hz, 2H), 7.74 (t, $J = 7.3$ Hz, 2H), 7.56 (t, $J = 7.4$ Hz, 2H), 4.36 (t, $J = 7.5$ Hz, 4H), 1.75–1.65 (m, 4H), 1.50–1.25 (m, 12H), 0.89 ppm (t, $J = 6.7$ Hz, 6H); ¹³C NMR (75 MHz, CDCl₃): $\delta = 162.63$, 157.13, 155.42, 148.05, 136.59, 135.91, 129.95, 129.11, 127.90, 127.71, 126.78, 117.70, 89.08, 42.33, 31.67, 26.70, 25.26, 22.70, 14.10 ppm; FAB-MS: m/z (%): 587.3 (100) [M+H]⁺; HRMS (FAB-MS): calcd for [C₃₆H₄₂N₈+H]⁺: 587.3611; found: 587.3611; elemental analysis (%) calcd for C₃₆H₄₂N₈: C 73.69, H 7.21, N 19.10; found: C 73.52, H 6.83, N 19.39.

Pyridine-2-carboxaldehyde [2-(9-anthracenyl)-pyrimidine-4,6-diyl]bis(methylhydrazone) (1h): A solution of 2-pyridinecarboxaldehyde **7a** (25 mg, 0.234 mmol) and **8e** (40 mg, 0.116 mmol) in EtOH (5 mL) was heated to reflux for 24 h. Then, the mixture was cooled and filtered. The precipitate was washed with EtOH and dried for 10 h under high vacuum: **1h** (33 mg, 54%). White solid. M.p. 343 °C. ¹H NMR (300 MHz, CDCl₃): $\delta = 8.64$ (d, $J = 4.4$ Hz, 2H), 8.55 (s, 1H), 8.26 (d, $J = 7.9$ Hz, 2H), 8.08 (s, 1H), 8.06 (d, $J = 9$ Hz, 2H), 7.92 (s, 2H), 7.90 (d, $J = 9$ Hz, 2H), 7.77 (td, $J = 7.6$, 1.2 Hz, 2H), 7.50–7.38 (m, 4H), 7.32–7.28 (m, 2H), 3.67 ppm (s, 6H); ¹³C NMR (75 MHz, CDCl₃): $\delta = 164.88$, 163.37, 155.23, 149.49, 137.15, 136.19, 134.82, 131.53, 129.55, 128.48, 127.61, 126.27, 125.79, 125.14, 123.08, 119.55, 87.13, 30.01 ppm; FAB-MS: m/z (%): 523.0 (100) [M+H]⁺; HRMS (FAB-MS): calcd for [C₃₂H₂₆N₈+H]⁺: 523.2359; found: 523.2345.

2-Acetylpyridine (pyrimidine-4,6-diyl)bis(methylhydrazone) (1i): A solution of 2-acetylpyridine **7b** (44 mg, 0.364 mmol) and **8a** (30 mg, 0.179 mmol) in EtOH (2 mL) was heated to reflux for 4 h. Then, the mixture was cooled, concentrated under vacuum to 0.2–0.3 mL, cooled on ice, and filtered. The precipitate was dried for 10 h under high vacuum: **1i** (45 mg, 67%). Yellow solid. M.p. 156 °C. ¹H NMR (300 MHz, CDCl₃): $\delta = 8.60$ (d, $J = 4.4$ Hz, 2H), 8.47 (s, 1H), 8.12 (d, $J = 8$ Hz, 2H), 7.53 (dt, $J = 7.8$, 1.2 Hz, 2H), 7.32–7.22 (m, 2H), 6.34 (s, 1H), 3.46 (s, 6H), 2.48 ppm (s, 6H); ¹³C NMR (75 MHz, CDCl₃): $\delta = 165.79$, 163.99, 156.95, 155.72, 148.76, 135.99, 124.33, 120.96, 87.35, 38.28, 16.28 ppm; FAB-MS: m/z (%): 375.2 (100) [M+H]⁺; HRMS (FAB-MS): calcd for [C₂₀H₂₂N₈+H]⁺: 375.2046; found: 375.2049; elemental analysis calcd (%) for C₂₀H₂₂N₈: C 64.15, H 5.92; found: C 64.02, H 5.62.

2-Phenylpyrimidine-4,6-dicarboxaldehyde bis[methyl(3-octadecyloxy-2-yl)hydrazone] (1m): A solution of **9b** (80 mg, 0.205 mmol) and **10b**

(21 mg, 0.099 mmol) in EtOH (2 mL) was heated to reflux for 4 h. Then, the mixture was cooled, concentrated under vacuum to 0.2–0.3 mL, and MeCN (0.5 mL) was added. The solution was cooled on ice, to precipitate the product. The precipitate was dried for 10 h under high vacuum: **1m** (40 mg, 42%). Yellow solid. M.p. 64°C. ¹H NMR (400 MHz, CDCl₃): δ = 8.46 (dd, *J* = 1, 7.9 Hz, 2H), 8.31 (s, 1H), 7.97 (dd, *J* = 1.2, 4.7 Hz, 2H), 7.60 (s, 2H), 7.52–7.45 (m, 3H), 7.20 (d, *J* = 7 Hz, 2H), 7.02 (dd, *J* = 4.7, 7.9 Hz, 2H), 3.88 (t, *J* = 7 Hz, 4H), 3.59 (s, 6H), 1.75–1.60 (m, 4H), 1.35–1.00 (m, 60H), 0.88 ppm (t, *J* = 6.7 Hz, 6H); ¹³C NMR (100 MHz, CDCl₃): δ = 164.41, 162.32, 148.49, 147.66, 138.68, 138.43, 131.91, 130.03, 128.36, 128.11, 120.76, 120.19, 107.90, 69.11, 35.32, 31.91, 29.69, 29.64, 29.62, 29.57, 29.39, 29.35, 29.25, 29.00, 25.79, 22.67, 14.10 ppm. FAB-MS: *m/z* (%): 959.8 (64) [M+H]⁺; HRMS (FAB-MS): calcd for [C₆₀H₉₄N₈O₂ + H]⁺: 959.7578; found: 959.7564.

Pyrimidine-4,6-diacetyl bis[methyl(pyridin-2-yl)hydrazone] (1n): A solution of **9a** (60 mg, 0.488 mmol) and **10c** (40 mg, 0.244 mmol) in EtOH (2 mL) was heated to reflux for 4 h. Then, the mixture was cooled and filtered. The precipitate was dried for 10 h under high vacuum: **1n** (41 mg, 45%). Yellow solid. M.p. 132°C. ¹H NMR (400 MHz, CDCl₃): δ = 9.23 (d, *J* = 1.2 Hz, 1H), 8.87 (d, *J* = 1.2 Hz, 1H), 8.30 (d, *J* = 3.8 Hz, 2H), 7.57–7.48 (m, 2H), 7.30 (d, *J* = 8.5 Hz, 2H), 6.83 (dd, *J* = 6.7, 5.6 Hz, 2H), 3.63 (s, 6H), 2.56 ppm (s, 6H); ¹³C NMR (100 MHz, CDCl₃): δ = 163.24, 160.06, 158.04, 154.85, 147.20, 137.15, 115.89, 112.81, 110.43, 39.21, 16.33 ppm; FAB-MS: *m/z* (%): 375.2 (100) [M+H]⁺; HRMS (FAB-MS): calcd for [C₂₀H₂₂N₈ + H]⁺: 375.2046; found: 375.2041; elemental analysis calcd (%) for C₂₀H₂₂N₈: C 64.15, H 5.92; found: C 63.77, H 5.91.

2-(9-Anthracenyl)-4,6-bis(1-methylhydrazino)pyrimidine (8e): Under magnetic stirring, 2-anthracenyl-4,6-dichloropyrimidine^[19] (100 mg, 0.308 mmol) was slowly added in portions to methylhydrazine (4 g, 10.853 mmol). The mixture was refluxed for 2 h under Ar. After the mixture had been allowed to cool, methylhydrazine was evaporated and the solid was dried under vacuum for 10 h: **8e** (quantitatively), NMR pure and so used without further purification. White solid. M.p. 302°C (decomp). ¹H NMR (400 MHz, CDCl₃): δ = 8.48 (s, 1H), 8.01 (d, *J* = 8.3 Hz, 2H), 7.86 (d, *J* = 8.8 Hz, 2H), 7.46–7.35 (m, 4H), 6.22 (s, 1H), 4.16 (s, large, 4H), 3.29 ppm (s, 6H); ¹³C NMR (100 MHz, CDCl₃): δ = 164.93, 164.69, 135.59, 131.54, 129.31, 128.30, 127.05, 126.41, 125.42, 124.97, 78.76, 40.03 ppm; FAB-MS: *m/z* (%): 345.2 (100) [M+H]⁺; HRMS (FAB-MS): calcd for [C₂₀H₂₀N₆ + H]⁺: 345.1841; found: 345.1836.

2-(1-Methylhydrazino)-3-octadecyloxy pyridine (9b): Under magnetic stirring, **11b** (200 mg, 0.524 mmol) was slowly added in portions to methylhydrazine (10 g, 217.391 mmol). The mixture was refluxed for 26 h under Ar. After the mixture had been allowed to cool, methylhydrazine was evaporated, K₂CO₃ (72 mg, 0.524 mmol) and CHCl₃ (20 mL) were added to the solid residue, and the mixture was stirred during 10 min. The liquid phase was filtered. The solid-liquid extraction procedure was repeated three times with CHCl₃ (without adding K₂CO₃), and the combined liquid fraction was evaporated: **9b** (quant.), NMR pure and so used without further purification. Yellowish solid. M.p. 51°C. ¹H NMR (400 MHz, CDCl₃): δ = 7.85 (dd, *J* = 4.9, 1.5 Hz, 1H), 7.04 (dd, *J* = 7.8, 1.5, 1H), 6.85 (dd, *J* = 4.9, 7.8 Hz, 1H), 3.99 (t, *J* = 6.5 Hz, 2H), 3.13 (s, 3H), 1.93–1.84 (m, 2H), 1.53–1.46 (m, 2H), 1.40–1.20 (m, 28H), 0.88 ppm (t, *J* = 6.3 Hz, 2H); ¹³C NMR (100 MHz, CDCl₃): δ = 154.18, 145.70, 137.96, 118.28, 117.51, 68.39, 43.70, 31.89, 29.67, 29.59, 29.55, 29.50, 29.33, 29.31, 29.13, 26.17, 22.65, 14.08 ppm; ES-MS: *m/z* (%): 392.38 (100) [M+H]⁺ = [C₂₄H₄₅N₃O + H]⁺.

2-Chloro-3-octadecyloxy pyridine (11b): 2-Chloro-3-hydroxypyridine (200 mg, 1.550 mmol), octadecylbromide (517 mg, 1.55 mmol), K₂CO₃ (430 mg, 3.110 mmol) and DMF (10 mL) were stirred for 8 h under Ar, at 65°C. After the mixture had been allowed to cool, the DMF was removed under vacuum, then water (20 mL) was added, and the solution was extracted with CHCl₃ (2 × 10 mL). The organic phase was evaporated and dried under vacuum for 10 h: **11b** (quantitatively), NMR pure and so used without further purification. White solid. M. p. 62°C (after purification by filtration on alumina; solvent CHCl₃). ¹H NMR (400 MHz, CDCl₃): δ = 7.96 (t, *J* = 3.1 Hz, 1H), 7.17 (d, *J* = 3.1 Hz, 2H), 4.02 (t, *J* = 6.6 Hz, 2H), 1.90–1.80 (m, 2H), 1.55–1.45 (m, 2H), 1.35–1.00 (m, 28H), 0.88 ppm (t, *J* = 6.8 Hz, 3H); ¹³C NMR (100 MHz, CDCl₃): δ = 151.29,

141.11, 140.21, 123.00, 120.02, 69.28, 31.91, 29.68, 29.64, 29.55, 29.51, 29.35, 29.26, 28.89, 25.89, 22.67, 14.10 ppm; ES-MS: *m/z* (%): 382.30 (100) [M+H]⁺ = [C₂₃H₄₀ClNO + H]⁺.

Pyridine-2-carboxaldehyde-(pyridin-2-yl)methylhydrazone (12): A solution of **7a** (52 mg, 0.488 mmol) and **9a** (60 mg, 0.488 mmol) in EtOH (3 mL) was heated to reflux for 3 h. Then, the mixture was cooled and water (5 mL) was added. The precipitate was dried for 10 h under high vacuum: **12** (90 mg, 87%). White solid. M. p. 105°C. ¹H NMR (400 MHz, CDCl₃): δ = 8.57 (ddd, *J* = 5.0, 1.5, 0.9 Hz, 1H), 8.24 (ddd, *J* = 5.0, 1.8, 0.9 Hz, 1H), 8.02 (d, *J* = 8 Hz, 1H), 7.76 (s, 1H), 7.74 (d, *J* = 8.5 Hz, 1H), 7.70 (td, *J* = 7.6, 1.5 Hz, 1H), 7.61 (ddd, *J* = 8.5, 7.3, 1.8 Hz, 1H), 7.18 (ddd, *J* = 7.6, 4.8, 1 Hz, 1H), 6.82 (ddd, *J* = 7, 5, 0.9 Hz, 1H), 3.70 ppm (s, 3H); ¹³C NMR (100 MHz, CDCl₃): δ = 157.43, 155.39, 149.20, 146.98, 137.50, 136.22, 134.70, 122.41, 119.24, 116.12, 110.03, 29.60 ppm; ES-MS: *m/z* (%): 213.10 (100) [M+H]⁺ = [C₁₂H₁₂N₄ + H]⁺; elemental analysis calcd (%) for C₁₂H₁₂N₄: C 67.90, H 5.70; found: C 67.92, H 5.73.

Synthesis of the metal complexes: The complexes were prepared by dissolution of the ligand in a solution consisting from the metal triflate and the solvent (CH₃CN, CH₃NO₂ or a mixture; CD₃CN, CD₃NO₂ for NMR observation). In the case of the grid, the stoichiometry metal ion: ligand must be respected; in the case of the rack, an excess of metal ion can be used. The chemical shift may slightly change depending on the solvent, on the concentration of the complex and, for the rack-type complexes, on the excess of metal ion.

1aGPb₄: The complex was obtained by mixing **1a** (2 mg, 5.78 μmol, 1 equiv) and Pb(OTf)₂ (2.92 mg, 5.78 μmol, 1 equiv) in CD₃CN (0.5 mL), which leads to complete dissolution of the ligand; yellow solution. ¹H NMR (400 MHz, CD₃CN): δ = 8.53 (s, 8H), 8.49 (s, 4H), 8.40 (d, *J* = 4.9 Hz, 8H), 7.98 (t, *J* = 7.3, 8H), 7.83 (d, *J* = 7.9 Hz, 8H), 7.27 (t, *J* = 6.1 Hz, 8H), 6.76 (s, 4H), 3.75 ppm (s, 24H); ES-MS: *m/z* calcd for [1a₄Pb₄(OTf)₂]²⁺ = [C₇₈H₇₂F₁₈N₃₂O₁₈Pb₄S₈]²⁺: 1555.1; found: 1554.8; calcd for [1a₄Pb₄(OTf)₃]³⁺ = [C₇₇H₇₂F₁₅N₃₂O₁₅Pb₄S₅]³⁺: 987.1; found: 986.5; calcd for [1a₄Pb₄(OTf)₄]⁴⁺ = [C₇₆H₇₂F₁₂N₃₂O₁₂Pb₄S₄]⁴⁺: 703.1; found: 702.9.

1aGZn₄: As described for **1aGPb₄**, with **1a** (2 mg, 5.78 μmol, 1 equiv) and Zn(OTf)₂ (2.10 mg, 5.78 μmol, 1 equiv) in CD₃CN (0.5 mL); orange solution. ¹H NMR (400 MHz, CD₃CN): δ = 8.57 (s, 8H, H_E), 7.97 (td, *J* = 7.8, 1.5 Hz, 8H), 7.93 (d, *J* = 5 Hz, 8H), 7.77 (d, *J* = 7.6 Hz, 8H), 7.36 (ddd, *J* = 7.6, 5.0, 0.9 Hz, 8H), 7.28 (s, 4H), 7.07 (s, 4H), 4.00 ppm (s, 24H).

1aLPb₂: The complex was obtained by mixing **1a** (2 mg, 5.78 μmol, 1 equiv) and Pb(OTf)₂ (7.3 mg, 14.45 μmol, 2.5 equiv) in CD₃CN (0.5 mL), which leads to complete dissolution of the ligand; yellow solution. ¹H NMR (400 MHz, CD₃CN): δ = 9.03 (s, 1H), 8.94 (d, *J* = 4.1 Hz, 2H), 8.74 (s, 2H), 8.23 (t, *J* = 7.7 Hz, 2H), 8.04 (d, *J* = 7.9 Hz, 2H), 7.81 (t, *J* = 6.1 Hz, 2H), 6.81 (s, 1H), 3.47 ppm (s, 6H); ¹H-¹H NOESY; ES-MS: calcd for [1aPb₂(OTf)₂]²⁺ = [C₂₀H₁₈F₆N₈O₆Pb₂S₂]²⁺: 530.0; found: 529.7.

1aLZn₂: As described for **1aLPb₂**, with **1a** (2 mg, 5.78 μmol, 1 equiv) and Zn(OTf)₂ (5.24 mg, 14.45 μmol, 2.5 equiv) in CD₃CN (0.5 mL); stirred overnight at 45°C; orange solution. ¹H NMR (400 MHz, CD₃CN): δ = 8.84 (s, 1H), 8.73 (d, *J* = 4.4 Hz, 2H), 8.30 (s, 2H), 8.27 (t, *J* = 7.7 Hz, 2H), 7.96 (d, *J* = 8 Hz, 2H), 7.81 (t, *J* = 6.4 Hz, 2H), 6.91 (s, 1H), 3.78 ppm (s, 6H).

1bLPb₂: As described for **1aLPb₂**, with **1b** (2 mg, 5.03 μmol, 1 equiv) and Pb(OTf)₂ (6.35 mg, 12.58 μmol, 2.5 equiv) in CD₃CN (0.5 mL); yellow solution. ¹H NMR (400 MHz, CD₃CN): δ = 9.11 (s, 1H), 8.97 (d, *J* = 4.1 Hz, 2H), 8.60 (s, 2H), 8.25 (td, *J* = 7.9, 1.5 Hz, 2H), 8.04 (d, *J* = 7.6 Hz, 2H), 7.88–7.82 (m, 2H), 6.47 (s, 1H), 6.10–5.95 (m, 1H), 5.34 (d, *J* = 10.8 Hz, 1H), 5.18 (d, *J* = 17.3 Hz, 1H), 4.93 ppm (s, 2H).

1cLPb₂: As described for **1aLPb₂**, with **1c** (3 mg, 6.17 μmol, 1 equiv) and Pb(OTf)₂ (7.81 mg, 15.43 μmol, 2.5 equiv) in CD₃CN (0.5 mL); yellow solution. ¹H NMR (400 MHz, CD₃CN): δ = 9.04 (s, 1H), 8.96 (d, *J* = 4.4 Hz, 2H), 8.73 (s, 2H), 8.27 (t, *J* = 7.6 Hz, 2H), 8.11 (td, *J* = 7.6, 1.2 Hz, 2H), 7.84 (dd, *J* = 7.3, 6.4 Hz, 2H), 6.58 (s, 1H), 4.29 (t, *J* = 8 Hz, 4H), 1.90–1.78 (m, 4H), 1.63–1.52 (m, 4H), 1.50–1.30 (m, 8H), 0.95 ppm (t,

$J = 6.9$ Hz, 6H); ES-MS: calcd for $[\mathbf{1cPb}_2(\text{OTf})_2]^{2+} = [\text{C}_{30}\text{H}_{38}\text{F}_6\text{N}_8\text{O}_6\text{Pb}_2\text{S}_2]^{2+}$: 600.1; found: 599.8.

1dLPb₂: As described for **1aLPb₂**, with **1d** (2 mg, 4.59 μmol , 1 equiv) and $\text{Pb}(\text{OTf})_2$ (5.80 mg, 11.46 μmol , 2.5 equiv) in CD_3CN (0.5 mL); yellow solution. ^1H NMR (400 MHz, CD_3CN): $\delta = 8.90$ – 8.80 (m, 4H), 8.27 (td, $J = 7.6$, 1.5 Hz, 2H), 8.09 (d, $J = 7.6$ Hz, 2H), 7.89 (d, $J = 7.9$ Hz, 2H), 7.86– 7.80 (m, 2H), 7.65 (d, $J = 7.9$ Hz, 2H), 6.88 (s, 1H), 3.84 (s, 6H), 2.57 ppm (s, 3H).

1eLPb₂: As described for **1aLPb₂**, with **1e** (2 mg, 4.48 μmol , 1 equiv) and $\text{Pb}(\text{OTf})_2$ (6.80 mg, 13.45 μmol , 3 equiv) in CD_3CN (0.5 mL); yellow solution. ^1H NMR (400 MHz, CD_3CN): $\delta = 9.21$ (s, 1H), 9.03 (s, 2H), 8.82 (d, $J = 8.5$ Hz, 2H), 8.52 (d, $J = 8.5$ Hz, 2H), 8.23 (d, $J = 7.9$ Hz, 2H), 8.16 (d, $J = 8.5$ Hz, 2H), 8.05 (t, $J = 7.6$ Hz, 2H), 7.85 (t, $J = 7.6$ Hz, 2H), 6.97 (s, 1H), 3.89 ppm (s, 6H).

1eLZn₂: As described for **1aLPb₂**, with **1e** (2 mg, 4.48 μmol , 1 equiv) and $\text{Zn}(\text{OTf})_2$ (4.88 mg, 13.45 μmol , 3 equiv) in CD_3CN (0.5 mL); yellow solution. ^1H NMR (400 MHz, CD_3CN): $\delta = 8.96$ (s, 1H), 8.84 (d, $J = 8.2$ Hz, 2H), 8.57 (d, $J = 8.8$ Hz, 2H), 8.50 (s, 2H), 8.20 (d, $J = 8.2$ Hz, 2H), 8.11 (t, $J = 7.6$ Hz, 2H), 8.06 (d, $J = 8.8$ Hz, 2H), 7.87 (t, $J = 7.6$ Hz, 2H), 7.02 (s, 1H), 3.89 ppm (s, 6H).

1fLPb₂: As described for **1aLPb₂**, with **1f** (2 mg, 3.22 μmol , 1 equiv) and $\text{Pb}(\text{OTf})_2$ (8.14 mg, 16.08 μmol , 5 equiv) in CD_3CN (0.5 mL); orange solution. ^1H NMR (400 MHz, CD_3CN): $\delta = 9.16$ (s, 1H), 9.05 (s, 2H), 8.77 (d, $J = 8.2$ Hz, 2H), 8.43– 8.38 (m, 2H), 8.16– 8.10 (m, 4H), 7.92 (d, $J = 8.5$ Hz, 2H), 7.89– 7.84 (m, 2H), 7.80– 7.69 (m, 8H), 7.28 (s, 1H), 4.02 ppm (s, 6H).

1gLPb₂: As described for **1aLPb₂**, with **1g** (2 mg, 3.41 μmol , 1 equiv) and $\text{Pb}(\text{OTf})_2$ (5.17 mg, 10.24 μmol , 3 equiv) in CD_3CN (0.5 mL); orange solution. ^1H NMR (300 MHz, CD_3CN): $\delta = 9.18$ (s, 1H), 8.98 (s, 2H), 8.81 (d, $J = 8.4$ Hz, 2H), 8.49 (d, $J = 8.7$ Hz, 2H), 8.30– 8.10 (m, 4H), 8.03 (td, $J = 7.7$, 1.2 Hz, 2H), 7.84 (t, $J = 7.1$ Hz, 2H), 6.70 (s, 1H), 4.38 (t, $J = 7$ Hz, 4H), 1.90– 1.80 (m, 4H), 1.65– 1.55 (m, 4H), 1.50– 1.40 (m, 8H), 0.95 ppm (t, 6H).

1gLZn₂: As described for **1aLPb₂**, with **1g** (2 mg, 3.41 μmol , 1 equiv) and $\text{Zn}(\text{OTf})_2$ (3.71 mg, 10.24 μmol , 3 equiv) in CD_3CN (0.5 mL); yellow solution. ^1H NMR (300 MHz, CD_3CN): $\delta = 9.04$ (s, 1H), 8.84 (d, $J = 8.2$ Hz, 2H), 8.56 (d, $J = 8.6$ Hz, 2H), 8.49 (s, 2H), 8.20 (d, $J = 7.3$ Hz, 2H), 8.15– 8.05 (m, 4H), 7.87 (t, $J = 7.6$ Hz, 2H), 6.80 (s, 1H), 4.38 (t, $J = 7.8$ Hz, 4H), 1.90– 1.80 (m, 4H), 1.65– 1.35 (m, 12H), 0.93 ppm (t, $J = 7$ Hz, 6H); ES-MS: calcd for $[\mathbf{1gLZn}_2(\text{OTf})_3]^+ = [\text{C}_{39}\text{H}_{42}\text{F}_9\text{N}_8\text{O}_9\text{Zn}_2\text{S}_3]^+$: 1164.8; found: 1165.0.

1hLPb₂: As described for **1aLPb₂**, with **1h** (2 mg, 3.83 μmol , 1 equiv) and $\text{Pb}(\text{OTf})_2$ (9.68 mg, 19.16 μmol , 5 equiv) in CD_3CN (0.5 mL); yellow solution. ^1H NMR (400 MHz, CD_3CN): $\delta = 9.07$ (s, 1H), 8.78 (s, 2H), 8.43 (d, 2H), 8.40– 8.35 (m, 2H), 8.19 (td, $J = 7.6$, 1.8 Hz, 2H), 8.04 (d, $J = 8.0$ Hz, 2H), 7.90– 7.65 (m, 8H), 7.11 (s, 1H), 3.91 ppm (s, 6H).

1iLPb₂: As described for **1aLPb₂**, with **1i** (2 mg, 5.53 μmol , 1 equiv) and $\text{Pb}(\text{OTf})_2$ (6.75 mg, 13.37 μmol , 2.5 equiv) in CD_3CN (0.5 mL); yellow solution. ^1H NMR (300 MHz, CD_3CN): $\delta = 8.95$ (d, $J = 4.5$ Hz, 2H), 8.81 (s, 1H), 8.35– 8.25 (m, 4H), 8.00– 7.87 (m, 2H), 6.54 (s, 1H), 3.73 (s, 6H), 2.69 ppm (s, 6H).

1iLZn₂: As described for **1aLPb₂**, with **1i** (2 mg, 5.53 μmol , 1 equiv) and $\text{Zn}(\text{OTf})_2$ (4.85 mg, 13.37 μmol , 2.5 equiv) in CD_3CN (0.5 mL); yellow solution. ^1H NMR (300 MHz, CD_3CN): $\delta = 8.78$ – 7.70 (m, 3H), 8.33 (td, $J = 7.8$, 1.6 Hz, 2H), 8.18 (d, $J = 8.1$ Hz, 2H), 7.87 (ddd, $J = 7.6$, 4.9, 1.1 Hz, 2H), 6.68 (s, 1H), 3.87 (s, 6H), 2.79 ppm (s, 6H).

1jGZn₄: As described for **1aLPb₂**, with **1j** (2 mg, 5.78 μmol , 1 equiv) and $\text{Zn}(\text{OTf})_2$ (2.10 mg, 5.78 μmol , 1 equiv) in CD_3CN (0.5 mL); orange solution. ^1H NMR (300 MHz, $\text{CD}_3\text{CN}/\text{CDCl}_3$, 4/1): $\delta = 8.55$ (s, 8H), 8.37 (s, 4H), 7.93 (td, $J = 8.1$, 1.7 Hz, 8H), 7.71 (s, 4H), 7.57 (d, $J = 5$ Hz, 8H), 7.41 (d, $J = 8.5$ Hz, 8H), 7.01 (dd, $J = 7.0$, 5.7 Hz, 8H), 3.88 ppm (s, 24H).

1jLPb₂: As described for **1aLPb₂**, with **1j** (2 mg, 5.78 μmol , 1 equiv) and $\text{Pb}(\text{OTf})_2$ (7.30 mg, 14.45 μmol , 2.5 equiv) in CD_3CN (0.5 mL); orange solution. ^1H NMR (400 MHz, CD_3CN): $\delta = 9.57$ (s, 1H), 8.59 (d, $J = 4.8$ Hz, 2H), 8.48 (s, 2H), 8.12 (s, 1H), 8.09 (t, $J = 8.9$ Hz, 2H), 7.57 (d, $J = 8.2$ Hz, 2H), 7.41 (t, $J = 6.3$ Hz, 2H), 3.75 ppm (s, 6H); ^{207}Pb NMR

(indirect observation): $\delta = 951.00$ ppm; ES-MS: calcd for $[\mathbf{1jLPb}_2(\text{OTf})_2]^{2+} = [\text{C}_{20}\text{H}_{18}\text{F}_6\text{N}_8\text{O}_6\text{Pb}_2\text{S}_2]^{2+}$: 530.0; found: 529.7.

1jLZn₂: As described for **1aLPb₂**, with **1j** (2 mg, 5.78 μmol , 1 equiv) and $\text{Zn}(\text{OTf})_2$ (5.24 mg, 14.45 μmol , 2.5 equiv) in CD_3CN (0.5 mL); yellow solution. ^1H NMR (300 MHz, $\text{CD}_3\text{CN}/\text{CDCl}_3$, 4/1): $\delta = 9.35$ (s, 1H), 8.45 (dd, $J = 1.2$, 5.4 Hz, 2H), 8.25– 8.10 (m, 5H), 7.56 (d, $J = 8.8$ Hz, 2H), 7.44 (dd, $J = 5.2$, 7.2 Hz, 2H), 3.77 ppm (s, 6H).

1kLPb₂: As described for **1aLPb₂**, with **1k** (2 mg, 4.74 μmol , 1 equiv) and $\text{Pb}(\text{OTf})_2$ (6.00 mg, 11.85 μmol , 2.5 equiv) in CD_3CN (0.5 mL); red solution. ^1H NMR (400 MHz, CD_3CN): $\delta = 8.64$ (s, 2H), 8.50 (d, $J = 4.7$ Hz, 2H), 8.18– 8.06 (m, 5H), 7.90– 7.83 (m, 3H), 7.63 (d, $J = 8.5$ Hz, 2H), 7.44 (t, $J = 6.3$ Hz, 2H), 3.78 ppm (s, 6H).

1lLPb₂: As described for **1aLPb₂**, with **1l** (2 mg, 4.93 μmol , 1 equiv) and $\text{Pb}(\text{OTf})_2$ (6.23 mg, 12.32 μmol , 2.5 equiv) in CD_3CN (0.5 mL); orange solution. ^1H NMR (300 MHz, CD_3CN): $\delta = 9.60$ (s, 1H), 8.68 (s, 2H), 8.60 (d, $J = 4$ Hz, 2H), 8.18 (s, 1H), 8.12– 8.03 (m, 2H), 7.72 (d, $J = 8.9$ Hz, 2H), 7.42 (dd, $J = 6.7$, 5.5 Hz, 2H), 4.48 (t, $J = 5.2$ Hz, 4H), 4.06 (t, $J = 6.0$ Hz, 4H), 3.65 ppm (s, large, 2H); FAB-MS: calcd for $[\mathbf{1lPb}_2(\text{OTf})_3]^+ = [\text{C}_{23}\text{H}_{22}\text{F}_9\text{N}_8\text{O}_{11}\text{Pb}_2\text{S}_3]^+$: 1269.0; found 1268.8; calcd for $[\mathbf{1lPb}_2(\text{OTf})_2\text{H}]^+ = [\text{C}_{22}\text{H}_{21}\text{F}_8\text{N}_8\text{O}_8\text{Pb}_2\text{S}_2]^+$: 1119.0; found 1118.8; ES-MS: calcd for $[\mathbf{1lPb}_2(\text{OTf})_2]^{2+} = [\text{C}_{22}\text{H}_{22}\text{F}_8\text{N}_8\text{O}_8\text{Pb}_2\text{S}_2]^{2+}$: 560.0; found 559.7.

1mGZn₄: As described for **1aLPb₂**, with **1m** (3 mg, 3.13 μmol , 1 equiv) and $\text{Zn}(\text{OTf})_2$ (1.14 mg, 3.13 μmol , 1 equiv) in CD_3CN (0.5 mL); red solution. ^1H NMR (400 MHz, $\text{CD}_3\text{CN}/\text{CDCl}_3$, 1/1): $\delta = 8.22$ (s, 4H), 8.12 (t, $J = 7.8$ Hz, 4H), 7.84 (s, 8H), 7.65 (t, $J = 7.2$ Hz, 4H), 7.45 (d, $J = 4.7$ Hz, 8H), 7.09 (t, $J = 7.6$ Hz, 4H), 6.99 (dd, $J = 7.8$, 5.1 Hz, 8H), 6.93 (d, $J = 5.1$ Hz, 8H), 5.88 (d, $J = 7.1$ Hz, 4H), 5.58 (d, $J = 7.0$ Hz, 4H), 4.10– 3.90 (m, 16H), 3.69 (s, 24H), 1.90– 1.80 (m, 16H), 1.60– 1.20 (m, 240H), 0.86 ppm (t, $J = 6.7$ Hz, 24H); ES-MS: m/z calcd for $[\mathbf{1m}_4\text{Zn}_4(\text{OTf})_6]^{2+} = [\text{C}_{246}\text{H}_{376}\text{N}_{32}\text{O}_{266}\text{F}_{18}\text{Zn}_4]^{2+}$: 2496.9, found 2496.2.

1mLPb₂: As described for **1aLPb₂**, with **1m** (3 mg, 3.13 μmol , 1 equiv) and $\text{Pb}(\text{OTf})_2$ (3.96 mg, 7.83 μmol , 2.5 equiv) in CD_3CN (0.5 mL); red solution. ^1H NMR (400 MHz, CD_3CN): $\delta = 8.65$ (s, 2H), 8.12– 8.02 (m, 5H), 7.86– 7.78 (m, 3H), 7.71 (d, $J = 8.4$ Hz, 2H), 7.50 (dd, $J = 8.4$, 5.1 Hz, 2H), 4.17 (t, $J = 6.4$ Hz, 4H), 3.86 (s, 6H), 1.93– 1.83 (m, 4H), 1.60– 1.20 (m, 60H), 0.87 ppm (t, $J = 7$ Hz, 6H).

1nLPb₂: As described for **1aLPb₂**, with **1n** (3 mg, 8.02 μmol , 1 equiv) and $\text{Pb}(\text{OTf})_2$ (10.14 mg, 20.05 μmol , 2.5 equiv) in CD_3CN (0.5 mL); red solution. ^1H NMR (400 MHz, CD_3CN): $\delta = 9.74$ (s, 1H), 8.48 (d, $J = 4.1$ Hz, 2H), 8.46 (s, 1H), 8.05 (t, $J = 7.7$ Hz, 2H), 7.42 (d, $J = 8.5$ Hz, 2H), 7.31 (t, $J = 6.3$ Hz, 2H), 3.76 (s, 6H), 2.79 ppm (s, 6H).

1nLZn₂: As described for **1aLPb₂**, with **1n** (2 mg, 5.53 μmol , 1 equiv) and $\text{Zn}(\text{OTf})_2$ (4.85 mg, 13.37 μmol , 2.5 equiv) in CD_3CN (0.5 mL); yellow solution. ^1H NMR (300 MHz, CD_3CN): $\delta = 9.42$ (d, $J = 1.1$ Hz, 1H), 8.42 (d, $J = 1.2$ Hz, 1H), 8.40 (ddd, $J = 5.5$, 1.8, 0.8 Hz, 2H), 8.17 (ddd, $J = 8.7$, 7.4, 1.8 Hz, 2H), 7.45 (d, $J = 8.7$ Hz, 2H), 7.40 (ddd, $J = 7.4$, 5.5, 0.8 Hz, 2H), 3.91 (s, 6H), 2.86 ppm (s, 6H); ES-MS: m/z calcd for $[\mathbf{1nZn}_2(\text{OTf})_3]^+ = [\text{C}_{23}\text{H}_{22}\text{N}_8\text{O}_9\text{S}_3\text{Zn}_2\text{F}_9]^+$: 952.5, found: 952.9.

2LPb₃: As described for **1aLPb₂**, with **2** (2 mg, 4.17 μmol , 1 equiv) and $\text{Pb}(\text{OTf})_2$ (11.60 mg, 22.94 μmol , 5.5 equiv) in CD_3CN (0.6 mL); light orange solution. ^1H NMR (500 MHz, CD_3CN): $\delta = 9.62$ (s, 1H), 9.08 (s, 1H), 8.96 (d, $J = 3.4$ Hz, 1H), 8.75 (s, 1H), 8.69– 8.56 (m, 2H), 8.49 (s, 1H), 8.24 (td, $J = 7.7$, 1.2 Hz, 1H), 8.22 (s, 1H), 8.14– 8.09 (m, 1H), 8.06 (d, $J = 7.8$ Hz, 1H), 7.83 (t, $J = 6.0$ Hz, 1H), 7.60 (d, $J = 8.2$ Hz, 1H), 7.42 (t, $J = 5.9$ Hz, 1H), 6.90 (s, 1H), 3.80 (s, 3H), 3.76 (s, 3H), 3.73 ppm (s, 3H).

3LPb₄: As described for **1aLPb₂**, with **3** (3 mg, 4.88 μmol , 1 equiv) and $\text{Pb}(\text{OTf})_2$ (11.11 mg, 21.98 μmol , 4.5 equiv) in CD_3CN (0.6 mL); light orange solution. ^1H NMR (400 MHz, CD_3CN): $\delta = 9.70$ (s, 1H), 9.09 (s, 2H), 8.96 (d, $J = 4.9$ Hz, 2H), 8.77 (s, 2H), 8.66 (s, 2H), 8.32 (s, 1H), 8.25 (td, $J = 7.9$, 1.8 Hz, 2H), 8.06 (d, $J = 7.9$ Hz, 2H), 7.86– 7.80 (m, 2H), 6.96 (s, 2H), 3.84 (s, 6H), 3.80 ppm (s, 6H); ^{207}Pb NMR (indirect observation): $\delta = 960.21$, 566.81 ppm.

3GPb₆: The complex was obtained by mixing **3** (2 mg, 2.99 μmol , 1 equiv) and $\text{Pb}(\text{OTf})_2$ (3.31 mg, 2.99 μmol , 1 equiv) in CD_3NO_2 (0.5 mL); stirred on magnetic stirrer overnight at 40–45°C; orange solution. ^1H NMR (400 MHz, CD_3NO_2): $\delta = 9.25$ (s, 4H), 8.96 (s, 8H), 8.95 (s,

4H), 8.92 (s, 8H), 8.73 (s, 4H), 8.64 (s, 8H), 8.61 (s, 8H), 8.58–8.53 (m, 16H), 8.36 (s, 4H), 8.34 (d, $J=5.0$ Hz, 8H), 8.22 (s, 8H), 8.02–7.86 (m, 32H), 7.26 (t, $J=6.4$ Hz, 8H), 7.19 (t, $J=6.2$ Hz, 8H), 6.97 (s, 8H), 6.91 (s, 8H), 3.98 (s, 24H), 3.94 (s, 24H), 3.87 (s, 24H), 3.81 ppm (s, 24H).

4LPb₆: As described for **1aLPb₂**, with **4** (3 mg, 3.40 μmol, 1 equiv) and Pb(OTf)₂ (11.17 mg, 22.10 μmol, 6.5 equiv) in CD₃CN (0.5 mL); light orange solution. ¹H NMR (500 MHz, CD₃CN/CD₃NO₂ 1/1): δ = 9.75 (s, 2H), 9.24 (s, 1H), 9.15 (s, 2H), 8.96 (d, $J=4.9$ Hz, 2H), 8.86 (s, 2H), 8.77 (s, 2H), 8.74 (s, 2H), 8.40 (s, 2H), 8.27 (td, $J=7.7, 1.4$ Hz, 2H), 8.10 (d, $J=7.7$ Hz, 2H), 7.87 (dd, $J=6.8, 5.2$ Hz, 2H), 7.18 (s, 1H), 7.05 (s, 2H), 3.93 (s, 6H), 3.91 (s, 6H), 3.87 ppm (s, 6H); ²⁰⁷Pb NMR (104.3 MHz, CD₃CN/CD₃NO₂ 1/1): δ = 1006.83, 602.06, 564.44 ppm.

5LPb₄: As described for **1aLPb₂**, with **5** (1.5 mg, 1.30 μmol, 1 equiv) and Pb(OTf)₂ (5.93 mg, 11.73 μmol, 9 equiv) in CD₃CN (0.5 mL); light orange solution. ¹H NMR (500 MHz, CD₃CN): δ = 9.72 (s, 3H), 9.19 (s, 2H), 9.11 (s, 2H), 8.96 (d, $J=4.8$ Hz, 2H), 8.77 (s, 2H), 8.76–8.67 (m, 6H), 8.37 (s, 1H), 8.35 (s, 2H), 8.25 (td, $J=7.6, 1.5$ Hz, 2H), 8.07 (d, $J=7.6$ Hz, 2H), 7.83 (ddd, $J=7.6, 5.2, 1.0$ Hz, 2H), 7.11 (s, 2H), 6.97 (s, 2H), 3.88 (s, 12H), 3.85 (s, 6H), 3.81 ppm (s, 6H).

6LPb₁₀: As described for **1aLPb₂**, with **6** (2 mg, 1.41 μmol, 1 equiv) and Pb(OTf)₂ (7.83 mg, 15.50 μmol, 11 equiv) in CD₃CN (0.5 mL); light orange solution. ¹H NMR (400 MHz, CD₃CN): δ = 9.74 (s, 2H), 9.72 (s, 2H), 9.21 (s, 3H), 9.13 (s, 2H), 8.94 (d, $J=4.7$ Hz, 2H), 8.75 (s, 2H), 8.70 (s, 6H), 8.65 (s, 2H), 8.37 (s, 2H), 8.35 (s, 2H), 8.24 (td, $J=7.5, 1.4$ Hz, 2H), 8.05 (d, $J=7.9$ Hz, 2H), 7.86–7.78 (m, 2H), 7.10 (s, 3H), 6.96 (s, 2H), 3.87 (s, 18H), 3.84 (s, 6H), 3.80 ppm (s, 6H).

12Pb: As described for **1aLPb₂**, with **12** (2 mg, 9.43 μmol, 1 equiv) and Pb(OTf)₂ (4.77 mg, 9.43 μmol, 1 equiv) in CD₃CN (0.5 mL); yellow solution. ¹H NMR (400 MHz, CD₃CN): δ = 8.70 (dd, $J=4.7$ Hz, 1H), 8.59 (s, 1H), 8.49 (d, $J=4.4$ Hz, 1H), 8.18 (td, $J=7.3, 1.2$ Hz, 1H), 8.02 (td, $J=8.8, 1.8$ Hz, 1H), 7.94 (d, $J=7.6$ Hz, 1H), 7.74 (t, $J=6.0$ Hz, 1H), 7.44 (8d, $J=8.8$ Hz, 1H), 7.29 (t, $J=6.3$ Hz, 1H), 3.67 ppm (s, 3H).

Structural interconversion experiments

Conversion of 1a into 1aGPb₄ and 1aLPb₂ (¹H NMR, 400 MHz): Ligand **1a** (1 mg, 2.89 μmol, 1 equiv) was dissolved in CDCl₃ (100 μL) and introduced in a NMR tube, CD₃CN (400 μL) was added and the NMR spectrum of the free ligand was recorded, after decantation of the amount of precipitated ligand. A solution was prepared by dissolving Pb(OTf)₂ (2.92 mg, 5.78 μmol, 2 equiv) in CD₃CN (30 μL), and 15 μL of this solution was added to the NMR tube solution, converting **1a** into **1aGPb₄** and producing the change of the color from colorless to pale yellow and the complete dissolution of the ligand. Further addition of the rest of the Pb(OTf)₂ solution (15 μL) leads to conversion of **1aGPb₄** into **1aLPb₂**. Further addition of Pb(OTf)₂ (0.5 equiv, 0.73 mg) caused only minor changes in chemical shift positions and lead to the spectrum **1aLPb₂** shown in Figure 13.

Acid–base neutralization modulated contractions of ligand 3 using Pb(OTf)₂ (¹H NMR, 400 MHz): Ligand **3** (1 mg, 1.63 μmol, 1 equiv) was dissolved in CDCl₃ (200 μL) and introduced in a NMR tube, then CD₃CN (200 μL) was added. A solution of Pb(OTf)₂ (3.29 mg, 6.52 μmol, 4 equiv) in CD₃CN (30 μL) was added to the NMR tube solution, producing the change of the color from yellow (free ligand) to orange (**3** → **3LPb₄**). Tren (1 μL, 0.95 mg, 6.52 μmol, 4 equiv) was added to the NMR tube solution with a syringe, producing the change of the color from orange to yellow (**3LPb₄** → **3**). TfOH (1.72 μL, 2.93 mg, 19.56 μmol, 12 equiv) was added to the NMR tube solution with a syringe, producing a change of the color of the solution from yellow to orange (**3** → **3LPb₄**). Et₃N (2.72 μL, 1.97 mg, 19.56 μmol, 12 equiv) was added to the NMR tube with a syringe, producing the change of color from orange to yellow, as well as the conversion of **3LPb₄** into **3**.

Acid–base neutralization modulated contractions of ligand 4 using Pb(OTf)₂ (¹H NMR, 400 MHz): Ligand **4** (1 mg, 1.13 μmol, 1 equiv) was dissolved in CDCl₃ (160 μL) and introduced in a NMR tube, then CD₃CN (240 μL) was added. A solution of Pb(OTf)₂ (3.73 mg, 7.37 μmol, 6.5 equiv) in CD₃CN (30 μL) was added to the NMR tube solution, producing the change of the color from yellow (free ligand color) to orange, as well as the conversion **4** → **4LPb₆**. Tren (1.15 μL, 1.08 mg, 7.37 μmol,

6.5 equiv) was added to the NMR tube solution with a syringe, producing a change of the color from orange to yellow, as well as the conversion **4LPb₆** → **4**. TfOH (1.95 μL, 3.32 mg, 22.11 μmol, 19.5 equiv) was added to the NMR tube solution with a syringe, producing a change of color of the solution from weak yellow to orange, as well as the conversion **4** → **4LPb₆**. Et₃N (3.1 μL, 2.23 mg, 22.11 μmol, 19.5 equiv) was added to the NMR tube with a syringe, producing the change of color from orange to yellow, as well as the conversion **4LPb₆** → **4**. Similar transformations were effected by using other **4**:Pb^{II} molar ratios such as 1:7 or 1:8. Consequently, in these cases, the amount of the other reagents used should be adapted. Depending on the quality of the reagents employed (tren, TfOH) and especially on their degree of hydration, their amounts should be slightly (5–10%) increased with respect to the theoretically calculated amount.

Crystal structure determinations: The crystals were obtained by diffusion-recrystallization by using the appropriate solvent and nonsolvent: CH₃NO₂/Et₂O for **1aLPb₂** and **1kLPb₂**; CH₃CN/*i*Pr₂O for **1eLZn₂** and **1fLPb₂**; CH₃CN/Et₂O for **1eLPb₂**, **1jLPb₂**, **1lLPb₂**, **1aGPb₄** and **3LPb₄**.

The crystals were placed in oil, and a single crystal was selected, mounted on a glass fiber and placed in a low-temperature N₂ stream (T = 173 K). The X-ray-diffraction data were collected on a Nonius-Kappa-CCD diffractometer with graphite monochromatized MoK_α radiation ($\lambda = 0.71073$ Å), ϕ scans, by means of a “ ϕ scan” type scan mode. The structures were solved by direct methods and refined (based on I^2 with all independent data) by full-matrix least-squares methods (OpenMoleN package).

Data for 1aLPb₂: Formula: C₉₁H₇₅F₄₈N₃₃O₅₁Pb₈S₁₆ = 4C₁₈H₁₈N₈Pb₂·16SO₃CF₃·CH₃NO₂·“C₂H₆O”; $M = 5529.32$ g mol⁻¹; crystal system: triclinic; space group: $P\bar{1}$; $a = 13.6176(2)$, $b = 16.4680(2)$, $c = 19.7257(3)$ Å; $\alpha = 67.347(5)^\circ$, $\beta = 89.399(5)^\circ$, $\gamma = 89.428(5)^\circ$; $V = 4082.0(1)$ Å³; $Z = 1$; color: yellow; crystal dimensions: $0.16 \times 0.12 \times 0.10$ mm³; $\rho_{\text{calcd}} = 2.249$ g cm⁻³; $F(000)$: 2604; $\mu = 8.564$ mm⁻¹; trans. min and max: 0.3411/0.4813; hkl limits: 0.19/–23,23/–27,27; limits($^\circ$): $2.5 \leq \theta \leq 30.04^\circ$; number of data measured: 23792; number of data with $I > 2\sigma(I)$: 20727; number of variables: 1101; $R = 0.0786$; $R_w = 0.2024$; GOF: 1.236; largest peak in final difference: 1.639 eÅ⁻³.

Data for 1eLPb₂: Formula: C₃₈H₃₄F₁₂N₁₂O₁₂Pb₂S₄ = C₂₆H₂₂N₈Pb₂·4CF₃SO₃·4CH₃CN; $M = 1621.38$ g mol⁻¹; crystal system: triclinic; space group: $P\bar{1}$; $a = 13.1193(2)$, $b = 13.9098(3)$, $c = 15.9317(3)$ Å; $\alpha = 91.901(5)^\circ$, $\beta = 113.845(5)^\circ$, $\gamma = 95.253(5)^\circ$; $V = 2640.13(13)$ Å³; $Z = 2$; color: yellow; crystal dimensions: $0.20 \times 0.10 \times 0.04$ mm³; $\rho_{\text{calcd}} = 2.04$ g cm⁻³; $F(000)$: 1556; $\mu = 6.638$ mm⁻¹; trans. min and max: 0.461/0.767; hkl limits: 0.18/–19,19/–22,20; $2.5 \leq \theta \leq 30.06^\circ$; number of data measured: 15408; number of data with $I > 3\sigma(I)$: 10551; number of variables: 721; $R = 0.041$; $R_w = 0.060$; GOF: 1.134; Largest peak in final difference: 1.642 eÅ⁻³.

Data for 1eLZn₂: Formula: C₇₄H₆₅F₂₄N₂₅O₂₄S₈Zn₄ = 2C₂₆H₂₂N₈Zn₂·8CF₃SO₃·7CH₃CN; $M = 2624.58$ g mol⁻¹; crystal system: triclinic; space group: $P\bar{1}$; $a = 12.5357(1)$, $b = 14.1927(2)$, $c = 15.4786(2)$ Å; $\alpha = 82.767(5)^\circ$, $\beta = 67.102(5)^\circ$, $\gamma = 88.631(5)^\circ$; $V = 2515.73(5)$ Å³; $Z = 1$; color: colorless; crystal dimensions: $0.18 \times 0.10 \times 0.10$ mm³; $\rho_{\text{calcd}} = 1.732$ g cm⁻³; $F(000)$: 1319.5; $\mu = 1.234$ mm⁻¹; trans. min and max: 0.862/0.888; hkl limits: 0.17/–19,19/–19,21; $2.5 \leq \theta \leq 30.06^\circ$; number of data measured: 15405; number of data with $I > 3\sigma(I)$: 10914; number of variables: 718; $R = 0.039$; $R_w = 0.059$; GOF: 1.099; largest peak in final difference: 0.622 eÅ⁻³.

Data for 1fLPb₂: Formula: C₅₀H₃₉F₁₂N₁₁O₁₂Pb₂S₄ = C₄₀H₃₀N₈Pb₂·4CF₃SO₃·3CH₃CN; $M = 1756.55$ g mol⁻¹; crystal system: triclinic; space group: $P\bar{1}$; $a = 12.8916(2)$, $b = 14.2089(2)$, $c = 17.5909(3)$; $\alpha = 84.233(5)^\circ$, $\beta = 88.660(5)^\circ$, $\gamma = 70.193(5)^\circ$; $V = 3016.06(12)$ Å³; $Z = 2$; color: orange; crystal dimensions: $0.16 \times 0.08 \times 0.03$ mm³; $\rho_{\text{calcd}} = 1.93$ g cm⁻³; $F(000)$: 1696; $\mu = 5.819$ mm⁻¹; trans. min and max: 0.573/0.830; hkl limits: –18,17/–20,19/–24,19; $2.5 \leq \theta \leq 30.06^\circ$; number of data measured: 25733; number of data with $I > 3\sigma(I)$: 9347; $I > 3\sigma(I)$; number of variables: 823; $R = 0.046$; $R_w = 0.054$; GOF: 1.317; largest peak in final difference: 1.517 eÅ⁻³.

Data for 1jLPb₂: Formula: C₁₃H₁₂F₆N₅O₆PbS₂ = 1/2C₁₈H₁₈N₈Pb₂·2CF₃SO₃·CH₃CN; $M = 719.59$ g mol⁻¹; crystal system: monoclinic; space group: C12c1; $a = 24.2087(4)$, $b = 8.7239(2)$, $c =$

22.1859(4) Å; $\beta = 108.849(5)^\circ$; $V = 4434.3(1) \text{ \AA}^3$; $Z = 8$; color: yellow; crystal dimensions: $0.14 \times 0.12 \times 0.10 \text{ mm}^3$; $\rho_{\text{calcd}} = 2.156 \text{ g cm}^{-3}$; $F(000)$: 2728; $\mu = 7.888 \text{ mm}^{-1}$; trans. min and max: 0.4047/1.5059; hkl limits: $-31, 31/-10, 11/-28, 28$; $2.5 \leq \theta \leq 27.88^\circ$; number of data measured: 9116; number of data with $I > 2\sigma(I)$: 4073; number of variables: 301; $R = 0.0314$; $R_w = 0.0960$; GOF: 1.068; largest peak in final difference: 1.558 e \AA^{-3} .

Data for 1kLPb₂: Formula: $\text{C}_{60}\text{H}_{50}\text{F}_{24}\text{N}_{18}\text{O}_{29}\text{Pb}_4\text{S}_8 = 2\text{C}_{24}\text{H}_{22}\text{N}_8\text{Pb}_2 \cdot 8\text{CF}_3\text{SO}_3 \cdot 2\text{CH}_3\text{NO}_2 \cdot \text{C}_2\text{H}_6\text{O}$; crystal system: monoclinic; space group: $P121/n1$; $a = 15.3338(2)$, $b = 15.7555(3)$, $c = 20.0979(3) \text{ \AA}$; $\beta = 102.298(5)^\circ$; $V = 4744.1(1) \text{ \AA}^3$; $Z = 2$; color: yellow; crystal dimensions: $0.10 \times 0.10 \times 0.08 \text{ mm}^3$; $\rho_{\text{calcd}} = 2.120 \text{ g cm}^{-3}$; $F(000)$: 2880; $\mu = 7.382 \text{ mm}^{-1}$; trans. min and max: 0.5256/0.5897; hkl limits: $-20, 20/-21, 19/-27, 27$; $2.5 \leq \theta \leq 29.12^\circ$; number of data measured: 21962; number of data with $I > 2\sigma(I)$: 7976; number of variables: 612; $R = 0.0632$; $R_w = 0.1757$; GOF: 0.998; largest peak in final difference: 1.894 e \AA^{-3} .

Data for 1lLPb₂: Formula: $\text{C}_{24}\text{H}_{20}\text{F}_{12}\text{N}_8\text{O}_{14}\text{Pb}_2\text{S}_4 = \text{C}_{20}\text{H}_{20}\text{N}_8$ ("OH")₂Pb₂·4CF₃SO₃; $M = 1415.10 \text{ g mol}^{-1}$; crystal system: orthorhombic; space group: $Fdd2$; $a = 42.9522(1)$, $b = 40.2922(4)$, $c = 9.4120(4) \text{ \AA}$; $V = 16288.8(7) \text{ \AA}^3$; $Z = 16$; color: orange; crystal dimensions: $0.10 \times 0.10 \times 0.08 \text{ mm}^3$; $\rho_{\text{calcd}} = 2.308 \text{ g cm}^{-3}$; $F(000)$: 10688; $\mu = 8.590 \text{ mm}^{-1}$; trans. min and max: 0.4805/0.5465; hkl limits: $-13, 13/-56, 56/-59, 60$; $2.5 \leq \theta \leq 30.00^\circ$; number of data measured: 11835; number of data with $I > 2\sigma(I)$: 5796; number of variables: 577; $R = 0.0349$; $R_w = 0.0973$; GOF: 1.016; largest peak in final difference: 1.880 e \AA^{-3} .

Data for 1aGPb₄: Formula: $\text{C}_{88}\text{H}_{84}\text{F}_{24}\text{N}_{36}\text{O}_{26}\text{Pb}_4\text{S}_8 = \text{C}_{72}\text{H}_{72}\text{N}_{32}\text{Pb}_4 \cdot 8\text{CF}_3\text{SO}_3 \cdot 4\text{CH}_3\text{CN} \cdot 2 \cdot \text{H}_2\text{O}$; $M = 3603.15 \text{ g mol}^{-1}$; crystal system: triclinic; space group: $P\bar{1}$; $a = 15.9249(2)$, $b = 20.3215(3)$, $c = 22.7099(4) \text{ \AA}$; $\alpha = 63.851(5)$, $\beta = 87.501(5)$, $\gamma = 72.198(5)^\circ$; $V = 6245.5(2) \text{ \AA}^3$; $Z = 2$; color: yellow; crystal dimensions: $0.08 \times 0.06 \times 0.06 \text{ mm}^3$; $\rho_{\text{calcd}} = 1.916 \text{ g cm}^{-3}$; $F(000)$: 3488; $\mu = 5.627 \text{ mm}^{-1}$; trans. min and max: 0.6617/0.7289; hkl limits: $0, 20/-24, 26/-29, 29$; $2.5 \leq \theta \leq 26.00^\circ$; number of data measured: 24404; number of data with $I > 2\sigma(I)$: 17988; number of variables: 1583; $R = 0.0586$; $R_w = 0.1647$; GOF: 1.253; Largest peak in final difference: 2.431 e \AA^{-3} .

Data for 3LPb₄: Formula: $\text{C}_{38}\text{H}_{30}\text{F}_{24}\text{N}_{16}\text{O}_{26}\text{Pb}_4\text{S}_8 = \text{C}_{30}\text{H}_{30}\text{N}_{16}\text{Pb}_4 \cdot 8\text{CF}_3\text{SO}_3 \cdot 4 \cdot \text{H}_2\text{O}$; $M = 2700.02 \text{ g mol}^{-1}$; crystal system: triclinic; space group: $P\bar{1}$; $a = 10.0990(1)$, $b = 13.9413(1)$, $c = 28.1295(4) \text{ \AA}$; $\alpha = 86.012(5)$, $\beta = 82.968(5)$, $\gamma = 88.094(5)^\circ$; $V = 3919.91(7) \text{ \AA}^3$; $Z = 2$; color: orange; crystal dimensions: $0.14 \times 0.10 \times 0.10 \text{ mm}^3$; $\rho_{\text{calcd}} = 2.288 \text{ g cm}^{-3}$; $F(000)$: 2532; $\mu = 8.917 \text{ mm}^{-1}$; trans. min and max: 0.3683/0.4692; hkl limits: $0, 14/-19, 19/-39, 39$; $2.5 \leq \theta \leq 30.04^\circ$; number of data meas.: 22147; Number of data with $I > 2\sigma(I)$: 13642; number of variables: 896; $R = 0.0851$; $R_w = 0.2763$; GOF: 1.022; largest peak in final difference: 2.444 e \AA^{-3} .

CCDC-229275 (1aLPb₂), CCDC-284971 (1eLPb₂), CCDC-284972 (1eLZn₂), CCDC-292586 (1fLPb₂), CCDC-292796 (1jLPb₂), CCDC-284970 (1kLPb₂), CCDC-284969 (1lLPb₂), CCDC-229276 (1aGPb₄) and CCDC-229277 (3LPb₄) contain the supplementary crystallographic data for this paper. These data can be obtained free of charge from the Cambridge Crystallographic Data Centre via www.ccdc.cam.ac.uk/data_request/cif.

Acknowledgements

We thank Prof. Dean Astumian for lively discussions on molecular motions and motors, Dr. Annie Marquis for helpful discussions concerning stability constants, Dr Lionel Allouche for NMR measurements, and Raymond Hueber for mass spectrometry analyses. A.-M. S. thanks le Ministère de la Recherche, de la Jeunesse et de la Technologie for a pre-doctoral fellowship.

- [1] a) Special issue: (Ed.: J. F. Stoddart): *Acc. Chem. Res.*, **2001**, *34*, 409–522; b) V. Balzani, A. Credi, F. M. Raymo, J. F. Stoddart, *Angew. Chem.* **2000**, *112*, 3484–3530; *Angew. Chem. Int. Ed.* **2000**,

39, 3348–3391; c) C. Dietrich-Buchecker, M. C. Jimenez-Molero, V. Sartor, J.-P. Sauvage, *Pure Appl. Chem.* **2003**, *75*, 1383–1393; d) *Molecular Motors* (Ed.: M. Schliwa), Wiley-VCH, **2003**.

- [2] a) D. J. Hill, M. J. Mio, R. B. Prince, T. S. Hughes, J. S. Moore, *Chem. Rev.* **2001**, *101*, 3893–4012; b) S. H. Gellman, *Acc. Chem. Res.* **1998**, *31*, 173–180; c) A. E. Rowan, R. J. M. Nolte, *Angew. Chem.* **1998**, *110*, 65–71; *Angew. Chem. Int. Ed.* **1998**, *37*, 63–68.
- [3] M. Barboiu, J.-M. Lehn, *Proc. Natl. Acad. Sci. USA* **2002**, *99*, 5201–5206.
- [4] a) G. S. Hanan, J.-M. Lehn, N. Kyritsakas, J. Fischer, *J. Chem. Soc. Chem. Commun.* **1995**, 765–766; b) D. M. Bassani, J.-M. Lehn, G. Baum, D. Fenske, *Angew. Chem.* **1997**, *109*, 1931–1933; *Angew. Chem. Int. Ed. Engl.* **1997**, *36*, 1845–1847; c) M. Ohkita, J.-M. Lehn, G. Baum, D. Fenske, *Chem. Eur. J.* **1999**, *5*, 3471–3481.
- [5] a) G. S. Hanan, D. Volkmer, U. S. Schubert, J.-M. Lehn, G. Baum, D. Fenske, *Angew. Chem.* **1997**, *109*, 1929–1931; *Angew. Chem. Int. Ed. Engl.* **1997**, *36*, 1842–1844; b) J. Rojo, F. J. Romero-Salguero, J.-M. Lehn, G. Baum, D. Fenske, *Eur. J. Inorg. Chem.* **1999**, 1421; c) A. M. Garcia, F. J. Romero-Salguero, D. M. Bassani, J.-M. Lehn, G. Baum, D. Fenske, *Chem. Eur. J.* **1999**, *5*, 1803–1808; d) M. Barboiu, G. Vaughan, R. Graff, J.-M. Lehn, *J. Am. Chem. Soc.* **2003**, *125*, 10257–10265; e) for a related type of [4×4] grid-type complex see: S. T. Onions, A. M. Frankin, P. N. Horton, M. B. Hursthouse and C. J. Matthews, *Chem. Commun.* **2003**, 2864–2865; f) M. Ruben, J.-M. Lehn and G. Vaughan, *Chem. Commun.* **2003**, *12*, 1338–1339; g) for a recent review on grid-type complexes, see M. Ruben, J. Rojo, F. J. Romero-Salguero, L. H. Uppadine, J.-M. Lehn, *Angew. Chem.* **2004**, *116*, 3728–3747; *Angew. Chem. Int. Ed.* **2004**, *43*, 3644–3662.
- [6] a) G. S. Hanan, C. R. Arana, J.-M. Lehn, D. Fenske, *Angew. Chem.* **1995**, *107*, 1191; *Angew. Chem. Int. Ed. Engl.* **1995**, *34*, 1122–1124; b) G. S. Hanan, C. R. Arana, J.-M. Lehn, G. Baum, D. Fenske, *Chem. Eur. J.* **1996**, *2*, 1292–1302; c) B. Hasenknopf, J. Hall, J.-M. Lehn, V. Balzani, A. Credi, S. Campagna, *New J. Chem.* **1996**, *20*, 725–730; d) P. Ceroni, A. Credi, V. Balzani, S. Campagna, G. S. Hanan, C. R. Arana, J.-M. Lehn, *Eur. J. Inorg. Chem.* **1999**, *9*, 1409–1414; e) A.-M. Stadler, F. Punteriero, S. Campagna, N. Kyritsakas, R. Welter, J.-M. Lehn, *Chem. Eur. J.* **2005**, *11*, 3997–4009.
- [7] K. M. Gardinier, R. G. Khoury, J.-M. Lehn, *Chem. Eur. J.* **2000**, *6*, 4124–4131.
- [8] a) J.-L. Schmitt, A.-M. Stadler, N. Kyritsakas, J.-M. Lehn, *Helv. Chim. Acta* **2003**, *86*, 1598–1624; b) J.-L. Schmitt, J.-M. Lehn, *Helv. Chim. Acta* **2003**, *86*, 3417–3426.
- [9] a) For metal ion binding by the tren ligand, see: S. G. Zipp, A. P. Zipp, S. K. Madan, *Coord. Chem. Rev.* **1974**, *14*, 29–45; b) A.-M. Stadler, N. Kyritsakas, J.-M. Lehn, *Chem. Commun.* **2004**, *18*, 2024.
- [10] For a "muscle"-type molecular mechanical process based on rotaxanes (and having an amplitude of about $85\text{--}65 \text{ \AA} = 20 \text{ \AA}$ ($\approx 30\%$), roughly the same extension factor as the natural muscles), see: a) M. C. Jimenez-Molero, C. Dietrich-Buchecker, J.-P. Sauvage, *Chem. Commun.* **2003**, *14*, 1613–1616; b) M. C. Jimenez, C. Dietrich-Buchecker, J.-P. Sauvage, *Angew. Chem.* **2000**, *112*, 3422–3425; *Angew. Chem. Int. Ed.* **2000**, *39*, 3284–3287; c) M. C. Jimenez-Molero, C. Dietrich-Buchecker, J.-P. Sauvage, *Chem. Eur. J.* **2002**, *8*, 1456–1466; d) M. C. Jimenez, C. Dietrich-Buchecker, J.-P. Sauvage, A. De Cian, *Angew. Chem.* **2000**, *112*, 1351–1354; *Angew. Chem. Int. Ed.* **2000**, *39*, 1295–1298.
- [11] a) S. T. Howard, *J. Am. Chem. Soc.* **1996**, *118*, 10269–10274; b) A. Göller, U.-W. Grummt, *Chem. Phys. Lett.* **2000**, *321*, 399–405; c) G. Corongiu, P. Nava, *Int. J. Quantum Chem.* **2003**, *93*, 395–404; d) G. Corongiu, P. Nava, unpublished *ab initio* computations; e) E. Ruiz, J.-M. Lehn, unpublished *ab initio* computations.
- [12] J. W. Canary, J. Xu, J. M. Castagnetto, D. Rentzeperis, L. A. Marky, *J. Am. Chem. Soc.* **1995**, *117*, 11545–11547.
- [13] M. Bos, W. E. van der Linden, *Anal. Chim. Acta* **1996**, *332*, 201–211.
- [14] a) H.-J. Buschmann, *Chem. Ber.* **1985**, *118*, 3408–3412; b) F. Arnaud-Neu, B. Spiess, M.-J. Schwing-Weill, *J. Chem. Res. (S)* **1982**, *1*, 10–11; c) Y. Inoue, G. W. Gokel, *Cation binding by macrocycles*, Marcel Dekker Inc., **1990**.

- [15] J. D. Badjić, V. Balzani, A. Credi, S. Silvi, J. F. Stoddart, *Science* **2004**, *303*, 1845–1849.
- [16] M. A. Baldo, G. Chessa, G. Marangoni, B. Pitteri, *Synthesis* **1987**, 720–723.
- [17] T. Sakamoto, T. Sakasai, H. Yamanaka, *Chem. Pharm. Bull.* **1981**, *29*, 2485–2490.
- [18] a) D. M. Bassani, J.-M. Lehn, *Bull. Soc. Chim. Fr.* **1997**, *134*, 897–906; b) A. J. Majeed, Ø. Antonsen, T. Benneche, K. Undenheim, *Tetrahedron* **1989**, *45*, 993–1006.
- [19] G. S. Hanan, U. S. Schubert, D. Volkmer, E. Riviere, J.-M. Lehn, N. Kyritsakas, J. Fischer, *Can. J. Chem.* **1997**, *75*, 169–182.
- [20] H. E. Gottlieb, V. Kotlyar, A. Nudelman, *J. Org. Chem.* **1997**, *62*, 7512.

Received: September 29, 2005

Revised: March 30, 2006